Parabolic resonances in 3 d.o.f. near integrable Hamiltonian systems

Anna Litvak-Hinenzon*
Vered Rom-Kedar
The Faculty of Mathematics and Computer Sciences
The Weizmann Institute of Science, POB 26, Rehovot 76100, Israel
litvak@maths.warwick.ac.uk, vered@wisdom.weizmann.ac.il

October 30, 2000

Keywords: Instabilities, Transport, Chaos.
PACS: 02.30.Hq,05.45.+b,92.60.E,52.25.F

Abstract

When an integrable 3 degrees of freedom (d.o.f.) Hamiltonian system, possessing an m-resonant ($m = 1$ or 2) normally parabolic torus is perturbed, a parabolic m-resonance occurs. Parabolic 1-resonances are persistent (without the use of external parameters) in near integrable n ($n \geq 3$) d.o.f. Hamiltonians. Other types of parabolic resonances are persistent in this class of systems as a low (one or two) co-dimension phenomena, and thus they are expected to appear in many applications. Analytical and numerical study of a phenomenological model containing parabolic resonances of various types reveals the differences between the dynamics appearing in 2 and 3 d.o.f. systems. The energy-momenta bifurcation diagram is developed as a tool for studying the global structure of such systems. The numerical study demonstrates that parabolic resonances are an unavoidable source of large and fast instabilities in typical 3 d.o.f. systems.

*Current address: Mathematics Institute, The University of Warwick, Coventry CV4 7AL, UK

1 Introduction

Two fundamental differences between the phase space structure of two and three d.o.f. near-integrable Hamiltonian systems have attracted much of the scientific interest in recent years. The first difference is that for the 3 d.o.f. case KAM tori do not bound phase space regions as they do in the 2 d.o.f. case and the second difference is that resonance surfaces intersect each other densely on almost all energy surfaces in the 3 d.o.f. case whereas in the 2 d.o.f. case they intersect each other only at the origin, on the zero energy surface (see [1, 2, 3]). The "Arnold Diffusion" (diffusion along resonances) and *diffusion across resonances* scenarios associated with these resonance webs were the focus of many recent works. Indeed, resonance interactions play a major role in the higher dimensional apparatus (see, for example [6], and references therein). Other differences clearly exist: For example, it is well known that the behavior near fixed points becomes more complex as the dimension of the system is increased. Here, we describe another pan of the complexity of phase space structure which appears in higher dimensional systems - the appearance of low-dimensional resonant tori with degenerate normal stability - we call such a structure *parabolic resonance (PR).* In this paper we discuss the appearance of PRs in three d.o.f. systems and in subsequent paper we discuss the higher dimensional cases. We devote much of the paper to describe the construction of bifurcation diagrams in the space of constant of motion. This generalizes the shaded energy-momentum diagram developed for the 2 d.o.f. systems in [16]. We propose that such a diagram, which presents global information (in phase-space and in energy) regarding the structures of the integrable system is essential for understanding the system behavior under small perturbation.

Systems which exhibit *parabolic resonances* appear in many applications; indeed, in [11] we prove that PRs are generic and *persistent*[1] in a class of n degrees of freedom (d.o.f.) near integrable Hamiltonian systems depending on p parameters provided $n \geq 2$ and $n + p \geq 3$. For example, PR was discovered while investigating a 2 d.o.f. model describing the motion of

[1] By persistent we mean physically that the phenomena is robust - small changes in the form of the integrable system (or the family of systems for phenomena of positive co-dimension) will not alter the results. Mathematically, this means that the systems are persistent on a C^1-open set under C^r ($r \geq 1$) perturbations of the class of integrable Hamiltonian systems of the form $H_0(x, y, I; \mu)$.

weather balloons on geopotential surfaces of the earth atmosphere [13, 16, 17]. In section 3 a 3 d.o.f. model extension of this model is discussed. Other examples where PRs appear are the Duffing equation with a k-torus attached to it (the tori represent the effect of neutral modes), and a reduction of the nonlinear Srödinger equation ([7] and references therein) to a six dimensional Hamiltonian ODE.

To understand the role of parabolic resonances, we briefly review the relevant results regarding the phase space structure of 3 d.o.f. near integrable Hamiltonians. Typically, in the completely integrable case the phase space is foliated by invariant tori on which quasi-periodic/periodic motion occurs. The subject of their persistence in near integrable Hamiltonian systems was extensively studied in this century; the KAM theory [2] assures that the majority of the maximal dimensional invariant tori, satisfying some non-degeneracy and Diophantine conditions, persist under small Hamiltonian perturbations (hereafter perturbation will always mean Hamiltonian perturbations). These invariant tori play a major role in 1 and 2 d.o.f. systems: The solutions of such perturbed systems are either confined on KAM tori or trapped between pairs of them, and hence cannot wander arbitrarily far in the phase space. The KAM theory is true for higher dimensional systems as well, but in 3 or more d.o.f., the co-dimension of the invariant tori on the energy surface is larger than one, hence they do not bound the motion in phase space.

A lower dimensional torus is a torus (here a circle or a 2-torus) with a vector of inner frequencies ω, of dimension smaller than the number of d.o.f., and a vector of multipliers (here four or two dimensional) which determines its stability. If the multipliers are purely imaginary, the normal frequencies vector Ω (here a two dimensional vector or a scalar) is constructed by taking the imaginary parts of one of each complex-conjugate pair [4]. Such lower dimensional tori persist under small perturbations if ω satisfies certain Diophantine conditions and if, additionally, either the tori are normally hyperbolic[2] [5] or they are normally elliptic[3] and (ω,Ω) are Diophantine [14]. A lower dimensional torus is said to be *normally parabolic* if it has at least one zero normal frequency. Maximal dimensional (here two-dimensional) *normally parabolic* tori [9] (together with a saddle-center bifurcation scenario)

[2]Hyperbolic lower dimensional invariant torus is a torus such that its multipliers have a non-zero real part.

[3]Elliptic lower dimensional tori are those with non-zero purely imaginary multipliers.

survive small Hamiltonian perturbations under Diophantine conditions on their inner frequencies (for normally parabolic circles, additional Diophantine conditions are required on the elliptic part of Ω [9]). Summarizing, in the typical near integrable case, normally elliptic, hyperbolic or parabolic lower dimensional tori persist on Cantor sets of action values consisting of the Diophantine frequency vectors. In the integrable case, there is a zero-dimensional dense set of actions on which resonant[4] tori reside. In 3 or more d.o.f. integrable Hamiltonian systems, the families of actions corresponding to resonant tori intersect on energy surfaces, creating a resonance web. Under small Hamiltonian perturbations the resonant tori break into resonant zones and orbits may drift along them far from their initial values (this possible scenario, called Arnold Diffusion, is still not well understood, see [2], and references therein). In previous works it has been shown that orbits which start in the vicinity of low dimensional resonant tori, exhibit under small perturbations intricate chaotic motion. See, for example, [7, 8] and references therein.

Parabolic resonance occurs in 2 d.o.f. systems when the integrable Hamiltonian possesses a parabolic circle of fixed points. Such a circle is persistent in a one parameter family of 2 d.o.f. integrable Hamiltonian systems. Numerical simulations of systems exhibiting a parabolic resonance, such as the atmospheric model mentioned above, show that perturbed orbits, starting in the vicinity of a parabolic circle of fixed points, exhibit chaotic behavior which combines hyperbolic homoclinic chaos and elliptic resonance type localizations, while the orbit slowly slides through bifurcations. Although these orbits appear to be chaotic, they stay relatively close to their initial values (though the instability here is stronger than near a hyperbolic resonance or near an elliptic resonance). In the flat parabolic resonance case, order one instabilities of perturbed orbits were observed. The large instabilities that were observed for the atmospheric model with realistic parameters value, correspond mathematically to a nearly flat parabolic resonance, and result in a relatively fast traveling of the weather balloons from the equator to the poles, see [17]. The *tangential parabolic resonance* models the near flat case, and it was proved in [15] that it is a co-dimension two phenomenon for 2 d.o.f. near integrable Hamiltonians. Furthermore, in [15] it was shown that the parabolic resonance, and the near flat parabolic resonance, appear in some common 2 d.o.f. physical models.

[4] A torus is said to be resonant if its frequencies are rationally dependent.

Here we study parabolic resonances in 3 d.o.f. systems. A *parabolic m-resonance* occurs when a small Hamiltonian perturbation is applied to an integrable 3 d.o.f. Hamiltonian system, which possesses a *normally parabolic m-resonant 2-torus* (namely, on the 2 dimensional torus m independent resonant conditions are satisfied and the normal frequency of the torus vanishes). Numerical experiments suggest that slightly perturbed orbits, starting near the parabolic resonant torus of the integrable system, exhibit complicated behavior and instabilities. If in addition to the existence of an m-resonant parabolic torus in the integrable system, the isoenergetic non-degeneracy condition fails so that a whole family of resonant tori exist on the same energy surface, the near integrable system exhibits a *flat parabolic m-resonance.* In such cases, order one instabilities of slightly perturbed orbits are observed in numerical simulations even in the 2 d.o.f. case [15]. This case may be viewed as the higher dimensional analogue to the stochastic web which appears in degenerate two-dimensional area-preserving maps [18].

The paper is ordered as follows. First, we construct the simplest model of a 3 d.o.f. system attaining a PR (using normal form techniques), and describe the construction of the energy-momenta diagrams which supply *global* information regarding the singular points in phase space, including the appearance of different kinds of PRs. We compare between the 2 and 3 d.o.f. cases, and demonstrate the different dynamical scenarios which are associated with the new mechanisms of PRs which appear in the 3 d.o.f. case. A 3 d.o.f. atmospheric model is constructed and used as a test case application for our results on the phenomenological model.

2 A phenomenological model.

The simplest model exhibiting PRs (and near flat PRs) in near integrable 3 d.o.f. Hamiltonian systems is constructed using normal form techniques. The conditions for existence of parabolic 1 and 2-resonant 2-tori are formulated for the integrable Hamiltonian, and an expansion near these conditions is made.

Consider a general near integrable 3 d.o.f. Hamiltonian system of the form: $H(r, s, u, v, p, q; \mu)$, where μ is a vector of parameters. The integrable part of this system has three constants of motion in involution ($F_0 = H_0, F_1, F_2$). For most values of F (regular values), action angle coordinates on the 3-tori they define may be introduced. Singular values of F, defined as values for which dF_i are point-wise linearly dependent, correspond to singular, smaller dimensional surfaces. Consider a region of phase space where only one such singular relation occurs. Then, a simplectic nonsingular change of variables $(r, s, u, v, p, q; \mu) \to (x, y, \theta_1, I_1, \theta_2, I_2; \mu)$ may be performed, to two action-angle coordinates I_1,I_2 and θ_1, θ_2 and an additional conjugate pair (x, y), for which the singularity occurs ($\nabla_{(x,y)} H_0 = 0$). The integrable part of the new Hamiltonian is independent of the angles (θ_1 and θ_2) [3] and we denote it by $H_0(x, y, I_1, I_2; \mu)$:

$$H(x, y, \theta, I; \mu, \varepsilon) = H_0(x, y, I; \mu) + \varepsilon H_1(x, y, \theta, I; \mu, \varepsilon),$$

Geometrically, the six dimensional phase space of this Hamiltonian may be described in the following way: A 2-torus, (with actions I_1, I_2 and angles θ_1, θ_2) is attached to each point of the (x, y) plane. If the point in the (x, y) plane is an equilibrium, the torus attached to it is an invariant torus with the same normal stability type as of this fixed point. The (x, y) plane is called *the normal plane*, since it determines the normal stability type of the 2-tori attached to it [14]. The motion on the 2-tori is either quasi-periodic (non-resonant) or periodic (resonant). By simplectic change of variables the condition $\langle k, \omega\rangle = 0$; $k \in \mathbb{Z}^2\backslash\{0\}$ for one resonance is replaced by vanishing of one of the frequencies. Hence, in these coordinates, the simplest near integrable Hamiltonian attaining a parabolic resonance is of the form:

$$\begin{aligned} H_0(x, y, I; \mu) &= \frac{y^2}{2} - I_1\frac{x^2}{2} + \eta\frac{x^3}{3} + \frac{x^4}{4} + \alpha_2 I_2 + (\frac{1}{2} + \alpha_1)\frac{I_1^2}{2} + \frac{I_2^2}{2} + \alpha_3 I_1 I_2, \\ H_1(x, y, \theta, I; \mu, \varepsilon) &= \sum_{i=1}^{2} \varepsilon_i f_i(x, I_1, I_2, k_i\theta_i), \qquad (1) \end{aligned}$$

where f_i $(i = 1, 2)$ are polynomials in x, y, I_1 and I_2, and are 2π periodic in their last argument. $\mu = (\alpha_1, \alpha_2, \alpha_3, \eta, k_1, k_2)$, with $\alpha_1, \alpha_2 \in \mathbb{R}$, $\alpha_3, \eta \geq 0$ (by rescaling), $k_i \in \mathbb{Z}_+$, and $0 \leq \varepsilon_i \ll 1$; $i = 1, 2$. The corresponding system is:

$$
\begin{aligned}
\dot{x} &= y, \\
\dot{y} &= I_1 x - \eta x^2 - x^3 - \sum_{i=1}^{2} \varepsilon_i \frac{\partial f_i(x, I_1, I_2, k_i\theta_i)}{\partial x}, \\
\dot{\theta}_1 &= -\frac{x^2}{2} + (\frac{1}{2} + \alpha_1) I_1 + \alpha_3 I_2 + \sum_{i=1}^{2} \varepsilon_i \frac{\partial f_i(x, I_1, I_2, k_i\theta_i)}{\partial I_1}, \\
\dot{I}_1 &= -\varepsilon_1 \frac{\partial f_1(x, I_1, I_2, k_1\theta_1)}{\partial \theta_1}, \\
\dot{\theta}_2 &= \alpha_2 + I_2 + \alpha_3 I_1 + \sum_{i=1}^{2} \varepsilon_i \frac{\partial f_i(x, I_1, I_2, k_i\theta_i)}{\partial I_2}, \\
\dot{I}_2 &= -\varepsilon_2 \frac{\partial f_2(x, I_1, I_2, k_2\theta_2)}{\partial \theta_2},
\end{aligned} \tag{2}
$$

By construction, the unperturbed system ($\varepsilon_i = 0$) possesses at the origin, O_{xyI} ($O_{xyI} \equiv \{(x, y, I_1, I_2) | (x, y, I_1, I_2) = (0, 0, 0, 0)\}$), a two dimensional normally parabolic 1-resonant torus ($\dot{\theta}_1 = 0$ and the (x, y) subsystem has a zero eigenvalue there) for $\alpha_2 \neq 0$, and a 2-resonant parabolic torus for $\alpha_2 = 0$ (in addition, $\dot{\theta}_2 = 0$ at the origin). More generally, $x = y = 0$ defines a four dimensional invariant surface consisting of a family of 2-tori $O_{xy}(I) = \{(x, y, I_1, I_2) | \quad x = y = 0\}$.

We assume that the phenomenological model is in the standard form for mechanical Hamiltonian systems which are integrable to quartic order, that the energy surfaces are compact in the (x, y) plane, and that the system undergoes a pitchfork bifurcation when the unfolding parameter η is set to zero. By simplectic change of variables (for the integrable part of the Hamiltonian) only the first action, I_1, governs the stability type of the invariant 2-tori, while the other action, I_2, together with the external parameter, α_2, governs the existence of resonances. Hence, fixing $\eta \equiv 0$, for $I_1 < 0$ the 2-torus at $O_{xy}(I)$ is elliptic, for $I_1 = 0$ it is parabolic, and for $I_1 > 0$ it is hyperbolic. When $I_1 > 0$, additional two elliptic tori, attached to an elliptic equilibrium at $(x, y) = (\pm\sqrt{I_1}, 0)$ are created. The system (2) is constructed such that for certain values of the parameters some unperturbed energy surfaces contain a whole family of normally elliptic (or hyperbolic) resonant 2-tori ending at a resonant parabolic torus. In such cases the iso-energetic non-degeneracy condition fails on this whole family of tori and large instabilities of near by perturbed orbits are expected to occur. The parameter values for which this degeneracy occur are: When $\alpha_1 = 0$, there exists a family of elliptic tori, corresponding to $(x,y) = (\pm\sqrt{I_1}, 0)$, emanating from a parabolic torus at $(x,y) = (0,0)$, all belonging to the same energy surface, and all resonant (creating a flat 1-PR). When $\alpha_2 = 0$ and $\alpha_1 = \alpha_3^2$ these tori become tori of fixed points (creating a flat parabolic 2-resonance). When $\alpha_1 = -0.5$, there exist a family of resonant elliptic tori and a family of resonant hyperbolic tori, meeting at a resonant parabolic torus, which all correspond to $(x,y) = (0,0)$ and all belong to the same energy surface. When $\alpha_2 = 0$ and $\alpha_1 = \alpha_3^2 - 0.5$ these tori become tori of fixed points.

The parameter η governs small asymmetric perturbations. When $\eta > 0$ and fixed, the system undergoes a saddle-center bifurcation and a transcritical bifurcation in I_1 (instead of the symmetric pitchfork bifurcation): For $I_1 < \frac{-\eta^2}{4}$ the (x,y) system possess only one equilibrium, at the origin, which is elliptic. When $I_1 = \frac{-\eta^2}{4}$ additional parabolic equilibrium at $(x,y) = (\frac{-\eta}{2}, 0)$ is created. For $\frac{-\eta^2}{4} < I_1 < 0$ a center is created at $(x,y) = (\frac{-\eta-\sqrt{\eta^2+4I_1}}{2}, 0)$, and a saddle is created at $(x,y) = (\frac{-\eta+\sqrt{\eta^2+4I_1}}{2}, 0)$ (in addition to the elliptic equilibrium at the origin). When $I_1 = 0$, the equilibrium at $(x,y) = (\frac{-\eta+\sqrt{\eta^2+4I_1}}{2}, 0)$ coincides with the origin and becomes parabolic. And, when $I_1 > 0$, the origin becomes hyperbolic and $(x,y) = (\frac{-\eta+\sqrt{\eta^2+4I_1}}{2}, 0)$ becomes elliptic. All these equilibria of the (x,y) plane correspond to invariant 2-tori which are of the same normal stability type as the corresponding equilibrium. The appearance of transcritical bifurcation follows from fixing $O_{xy}(I)$ to be invariant for all I. Our preliminary study suggests that the system exhibits qualitatively different behavior for some values of $\eta > 0$. Here we treat only the symmetric case $\eta = 0$.

In appendix A we formulate the conditions for the appearance of a parabolic resonance, from which we had constructed the phenomenological model. We stress that the ability to arrange a model which exhibits many types of PRs is not accidental - it follows from our results regarding the persistence/low co-dimensionality of these mechanisms of instabilities. Next, the global structure of the 3 d.o.f. system is described and in the following subsection numerical studies of the near-integrable system are presented.

2.1 The integrable system - bifurcation diagrams in the space of constants of motion

To fully understand all possible behavior of the integrable 3 d.o.f. system (2) we construct bifurcation diagrams in the space of constants of motion. Such diagrams reveal the critical energy levels and phase space regions in which strong instabilities arising from the perturbation are expected. In these diagrams the allowed regions of motion and the type of motion which occur are indicated. Different types of motion are necessarily divided by singular surfaces. Further information regarding the frequencies are inserted, with the understanding that these play a crucial role when the perturbation is applied.

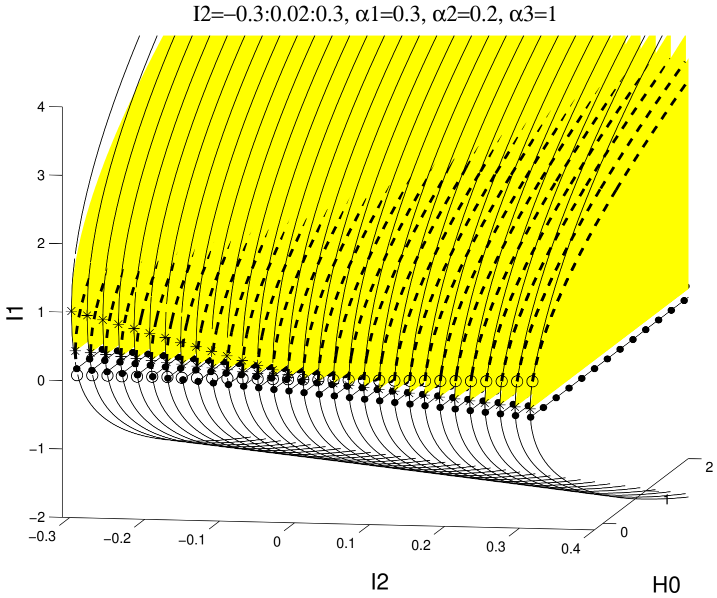

Figure 1: Energy-actions bifurcation diagram.
—— : elliptic 2-tori; $- - -$: hyperbolic 2-tori (and separatrices); 'o': parabolic 2-tori; $**$, $- \cdot - \cdot -$: resonances; Shaded volume: back-flow.

Such a bifurcation diagram is presented in figure 1. The axes of the figure are the energy, H_0 (more generally, the unperturbed Hamiltonian, where the full Hamiltonian is conserved under perturbation), and the actions of the 2-tori, I_1 and I_2 (more generally, the conjugate actions to the resonant terms in the perturbed Hamiltonian). A regular point in the allowed region of motion corresponds to one or two 3−tori, with a 3 dimensional frequency vector, $(\omega_1, \omega_2, \omega_3) = (\Omega(H_0, I), \omega(H_0, I))$, for the motion in the (x, y) plane and the (I, θ) planes respectively; a singular point of the (x, y) plane corresponds to an isolated invariant 2-torus, with a two dimensional vector of inner frequencies, $\omega(H_0, I) = (\omega_2, \omega_3) = (\dot{\theta}_1(I), \dot{\theta}_2(I))$. The normally elliptic and parabolic invariant 2-tori have a normal frequency, $\omega_1 = \Omega(I)$, while for normally hyperbolic 2-tori the normal frequency (and hence ω_1) cease to exist. The singular surface corresponding to the stable (elliptic) equilibria of the (x, y) plane (a normally elliptic 2−torus) are denoted by solid curves, each curve corresponds to a fixed value of I_2. These singular surfaces of normally elliptic 2−tori supply the boundary of the allowed region of motion. The singular surface corresponding to the unstable (hyperbolic) equilibria and *separatrices* are denoted by a manifold of dashed curves. Above the dashed curve each regular point corresponds to two 3−tori, whereas below it only one 3-torus is associated with each (H_0, I) value. Hence, the normally hyperbolic tori are interior and create a topological nontrivial deformation of the energy surface. Correspondingly, each point on the upper solid curves corresponds to *two* elliptic equilibria at $(x, y) = (\pm\sqrt{I_1}, 0)$ (hence, beginning at the dashed curve, the energy surface branches, arriving at two parallel solid curves which are identified in the figure). The parabolic 2−tori are in the meeting line between the solid and dashed surfaces, and are marked by a circle on each I_2 slice. Note that each one of the parabolic tori in this figure resides on a different energy surface.

In our representation, elliptic equilibria in the (x, y) plane supply the boundaries to the energy surfaces of the full system (it follows from [3], page 102). To find these boundaries, equation (1) is solved at these equilibria points for the first action, I_1, as a function of the other two constants of motion, H_0 and I_2, see appendix B for details. The result of these calculations are the location of the equilibria manifolds (which depend non-trivially on the parameters, see appendix B). The stability of these equilibria in the (x, y) plane defines the normal stability of the tori on the equilibria manifolds. We have thus demonstrated how the normal stability of the lower dimensional tori are represented in the diagram. In figures 5 - 8 the domains of definition of equation (1) is shown by vertical lines[5]. Hence, the above simple procedure

[5]In the three dimensional bifurcation diagram figure 1 the vertical lines were omitted for the convenience of the viewer, and the domain where motion is allowed in this figure is inside the parabola created by the upper and lower manifolds of solid curves (which refer

reveals all the possible topological distinct types of integrable level sets and their stability.

Furthermore, recall that under a small conservative perturbation the motion may spread along a single perturbed energy surface. Slicing the five dimensional energy surface at different angles, corresponds to moving across a small range of unperturbed energy surfaces. Hence, their boundaries supply a simple upper bound on the extend of the instability in the actions directions, see for example, figure 17. For our model we observe a wide variety of possibilities for the dependence of the allowed regions of motion on H_0, I_1, I_2, see Appendix B for details. In particular, for a fixed I_2, the energy surfaces are always bounded from below in I_1 direction by an elliptic equilibrium. When $-0.5 < \alpha_1 < 0$ the motion is unbounded from above in I_1 direction for any value of I_2 (see for example figure 7), and when $\alpha_1 = 0$ the motion is unbounded from above for $I_2 \leq 0$ (see for example figure 6:b,c). In all the other cases motion is bounded from above in I_1 direction by an elliptic equilibrium (see figures 1, 5 and 6:a). Hence, in some cases there is no bound on the growth of the action.

Next we address the appearance of resonances. Generally, resonances $\langle k, (\Omega, \omega) \rangle = 0$ appear in this diagram as two dimensional surfaces, intersecting each energy level by a curve. A full set of these curves creates a resonance web on each energy surface. Resonance surface information, for resonances of the maximal dimensional 3-tori, may be added to this diagram by averaging along the motion in the (x, y) plane to compute the frequencies $\omega_1 = \Omega$ and ω_2 (ω_3 is simply $\dot{\theta}_2(I) = \alpha_2 + I_2 + \alpha_3 I_1$). An example of such a resonance curve, corresponding to vanishing of ω_2 on 3-tori of one fixed energy surface, is presented in figure 2B as a line of asterisks. Special resonances may be directly found: The $(0, 0, 1)$ resonances, corresponding to vanishing of the frequency in the I_2 direction ($\omega_3 = \dot{\theta}_2(I) = 0$) are marked by a surface of dotted lines. The $(0, 1, 0)$ resonance surface corresponding to vanishing of the frequency in the I_1 direction intersect the singular invariant 2-torus surfaces at the curve of asterisks (on which $\omega_2 = \dot{\theta}_1(I) = 0$). In figure 1, it is seen that the line of circles, corresponding to the normally parabolic 2-tori ($I_1 = 0$) is crossed by the $(0, 1, 0)$-resonance curve of asterisks (only) at $I_2 = 0$, and by the $(0, 0, 1)$-resonance surface of dotted lines (only) at $I_2 = -\alpha_2 = -0.2$. As the normal frequency, $\omega_1 = \Omega$, vanishes on normally parabolic tori, nor-

to the elliptic equilibria points in the (x, y) plane).

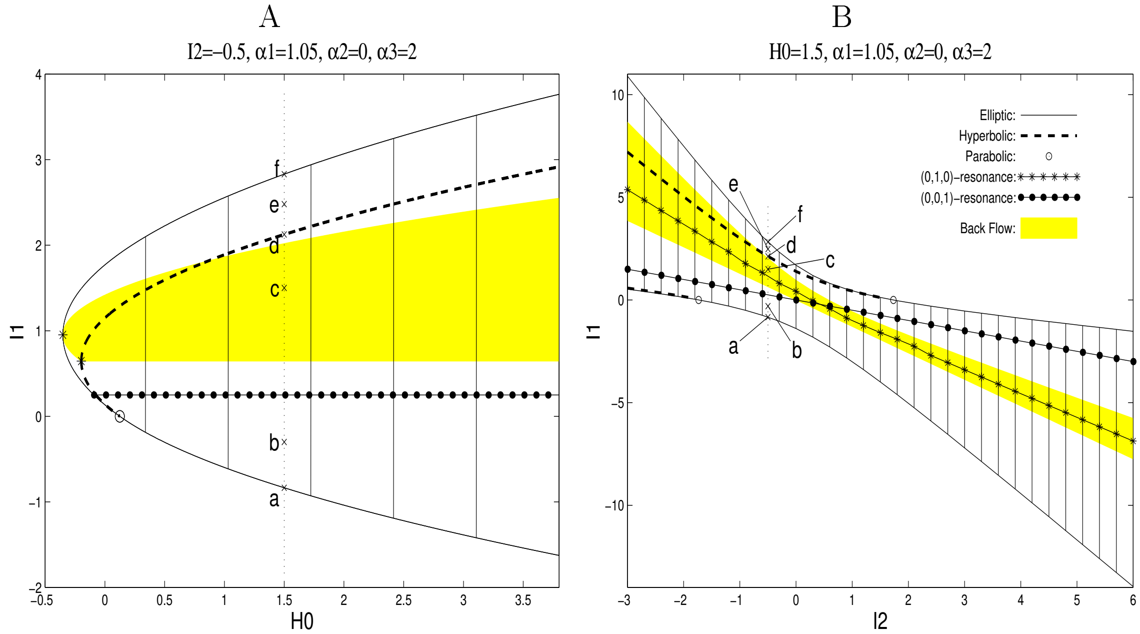

Figure 2: 2-d Slices of the 3-d energy-actions bifurcation diagram.
A: $I_2 = -0.5$ B: $H_0 = 1.5$.

mally parabolic tori are a-priori $(1, 0, 0)$-resonant. Hence, when the $(0, 1, 0)$-resonance surface intersects a parabolic 2-torus, it corresponds to occurrence of the *double* $\{(1, 0, 0), (0, 1, 0)\}$-resonance, and when the $(0, 0, 1)$-resonance surface intersects a parabolic 2-torus, it corresponds to occurrence of the *double* $\{(1, 0, 0), (0, 0, 1)\}$-resonance. When $\alpha_2 = 0$, the curve of asterisks, the surface of dotted lines and the line of circles all intersect in one point, corresponding to a 2-resonant normally parabolic torus, an event which correspond to occurrence of the *triple* $\{(1, 0, 0), (0, 1, 0), (0, 0, 1)\}$-resonance (see, for example, figures 8c and 9). All other resonant parabolic tori in figure 1 have weaker resonances (larger $|k|$ values) with respect to their *inner frequencies*. Therefore, the instabilities in the near integrable system (described in the following sections), which are a result of parabolic resonances, correspond to cross resonance diffusion. See [11] for a discussion on the place and role of parabolic resonant tori in the resonance web.

Another dynamical feature of interest is the possible existence of a back-flow in θ_1, namely a non-monotonic dependence of θ_1 on t, see figure 4. The regions where $\dot{\theta}_1$ changes sign along orbits are colored by a light gray in the

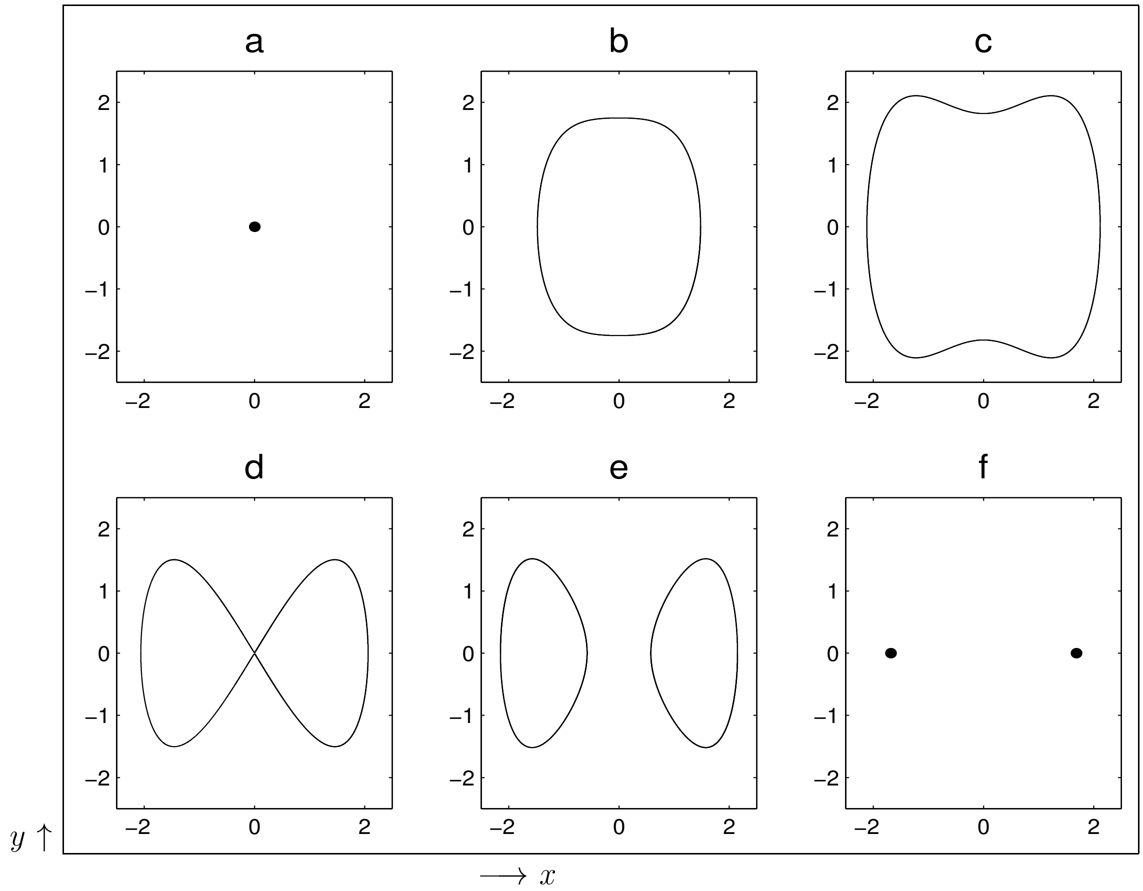

Figure 3: Orbit structure in the (x, y) plane.
$H_0 = 1.5$, $I_2 = 0.5$, and I_1 values at subfigures a-f are as indicated in figure 2; $\alpha_1 = 1.05$, $\alpha_2 = 0$, $\alpha_3 = 2$.

bifurcation diagrams (see figures 1, 2, 5, 6 and 7). Such a dynamical feature (detecting instantaneous zeroes of $\dot{\theta}_1$) may be found easily (see appendix C and table 2).The significance of this region is three-folded. First, only in a region where back-flow occurs the second frequency may vanish (equivalently, a $(0, 1, 0)$ resonance may appear). Second, when a back-flow occurs along a separatrix the usual transport mechanism associated with separatrix splitting must be modified. This scenario appears when the light grey shaded region in the energy-actions bifurcation diagrams covers the dashed hyperbolic equilibria curve. Finally, when $\dot{\theta}_1$ vanishes identically on a lower dimensional invariant torus, a $(1,0)$ resonance occurs with respect to the inner frequencies of the torus. Hence the intersection of the light grey volume with the equilibria surfaces consists of resonant lower dimensional tori which are indicated by asterisks in figures 1 - 9.

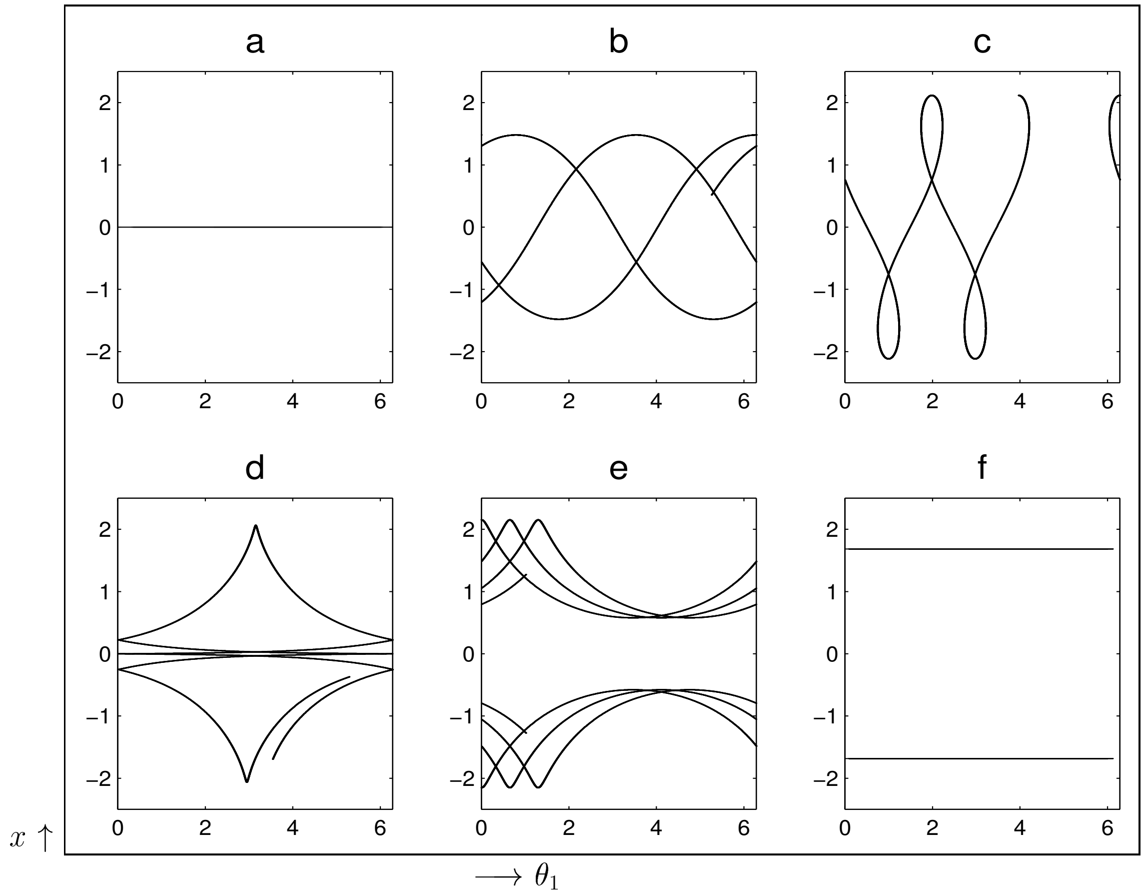

Figure 4: Orbit structure in the (θ_1, x) plane.
$H_0 = 1.5$, $I_2 = 0.5$, and I_1 values at subfigures a-f are as indicated in figure 2; $\alpha_1 = 1.05$, $\alpha_2 = 0$, $\alpha_3 = 2$. **c:** Back-flow.

The equilibrium surfaces and the phase information encoded in the bifurcation diagram allows one to extract complete description of the integrable motion. For clarity, by fixing I_2, we present isolated slices of the three dimensional bifurcation diagrams of the energy-actions space (figures 2A, and 5 - 8). The vertical solid lines in these figures denote the region of allowed motion.

Consider figure 2A, in which $I_2 = -0.5$. The energy surface with $H_0 = 1.5$ intersects this diagram at the light vertical dotted line. Alternatively, a slice of the bifurcation diagram in the (I_2, I_1) plane at the corresponding energy value $H_0 = 1.5$, is presented in figure 2B, with the corresponding light dotted vertical line denoting the intersection with the slice $I_2 = -0.5$. The points denoted by **a,b,c,d,e,f** on these lines, correspond to the six different types of orbits appearing on this energy surface at $I_2 = -0.5$. The corresponding six different types of motion in the (x, y) and (θ_1, x) planes are presented in the figures 3 and 4, respectively. The point **a** corresponds to one elliptic equilibrium in the (x, y) plane, hence to one normally elliptic 2-torus in the six dimensional phase space. The point **b** corresponds to a periodic orbit in the (x, y) plane (hence to a non-resonant 3-torus, which is densely covered by this orbit), which encircles the origin, and on which $\dot{\theta}_1$ does not change sign (since it is located in an unshaded region). The point **c** is in the shaded region hence it corresponds to a larger periodic orbit which encircles the origin in the (x, y) plane and exhibits back-flow in θ_1 (topologically it is indistinguishable from **b**, yet see figure 4c). The point **d** corresponds to an hyperbolic equilibrium and its separatrix in the (x, y) plane, hence to an invariant normally hyperbolic 2-torus and its corresponding three dimensional stable and unstable manifolds. The point **e** corresponds to two 3-tori, and the point **f** corresponds to two isolated invariant normally elliptic 2-tori. The motion for initial conditions with different energies and actions can be now read-off from figure 2 or its three-dimensional extension.

We regress to supply a few more details regarding the appearance of strong resonances. In particular, we demonstrate that geometrical features of the bifurcation diagram have dynamical significance.

In the integrable system (2), $\dot{\theta}_1$ vanishes on a lower dimensional invariant torus in two cases. The first case occurs when:

$$\dot{\theta}_1|_{O_{xy}} = \frac{\partial H_0}{\partial I_1}|_{(x,y)=(0,0)} = 0. \tag{3}$$

Graphically, this means that the resonance occurs exactly at the fold of the surface in the I_1 direction. In other words, for any fixed I_2, the I_1 which solves (3) is a local extrema of the energy value of the equilibria curves, see figures 1 - 9. It can be easily verified that this observation is correct even when the equilibria position depends on the actions[6]. These resonant lower

[6] For example, defining $G(I) = H_0(x(I), y(I), I)$, where $(x(I), y(I))$ are the equilibrium

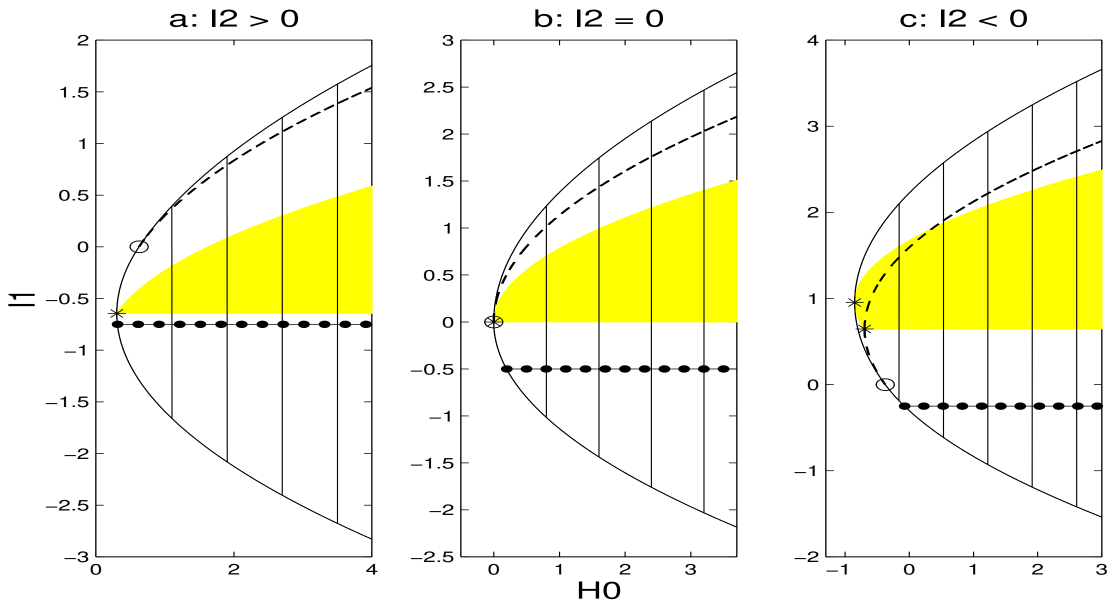

Figure 5: Slices of the energy-actions bifurcation diagram for $\alpha_1 > 0$.
$\alpha_1 = 1.05, \alpha_2 = 1, \alpha_3 = 2$. **a:** $I_2 = 0.5$; **b:** $I_2 = 0$; **c:** $I_2 = -0.5$
Vertical lines: regions of allowed motion, ——: elliptic 2-tori; $---$: hyperbolic 2-tori (and separatrices); 'o': parabolic 2-tori; $**$, $-\cdot-\cdot-$: resonances; Shaded volume: backflow.

dimensional tori are indicated by an asterisk in the bifurcation diagrams.

Equation (3) holds for:

$$I_{2_{res1}}(I_1) = -\frac{1+2\alpha_1}{2\alpha_3} I_1, \tag{4}$$

for any value of I_1. Hence, the corresponding resonant tori may be of any stability type, depending on the value of I_1. In particular, since $I_{2_{res1}}(0) = 0$, the 1-resonant 2-torus O_{xyI} is normally parabolic, and is therefore indicated by both asterisk and a circle in figure 8:a. In section 2.2 this parabolic 1-resonance is referred to as 1-PR in I_1 direction.

The second case occurs when:

$$\dot{\theta}_1|_{ell} = \frac{\partial H_0}{\partial I_1}|_{(x,y)=(\pm\sqrt{I_1},0)} = 0. \tag{5}$$

solution, we see that $\frac{\partial G}{\partial I_1} = \frac{\partial H_0}{\partial I_1}|_{(x(I),y(I),I)}$ because $\nabla_{xy} H_0|_{(x(I),y(I),I)} = 0$.

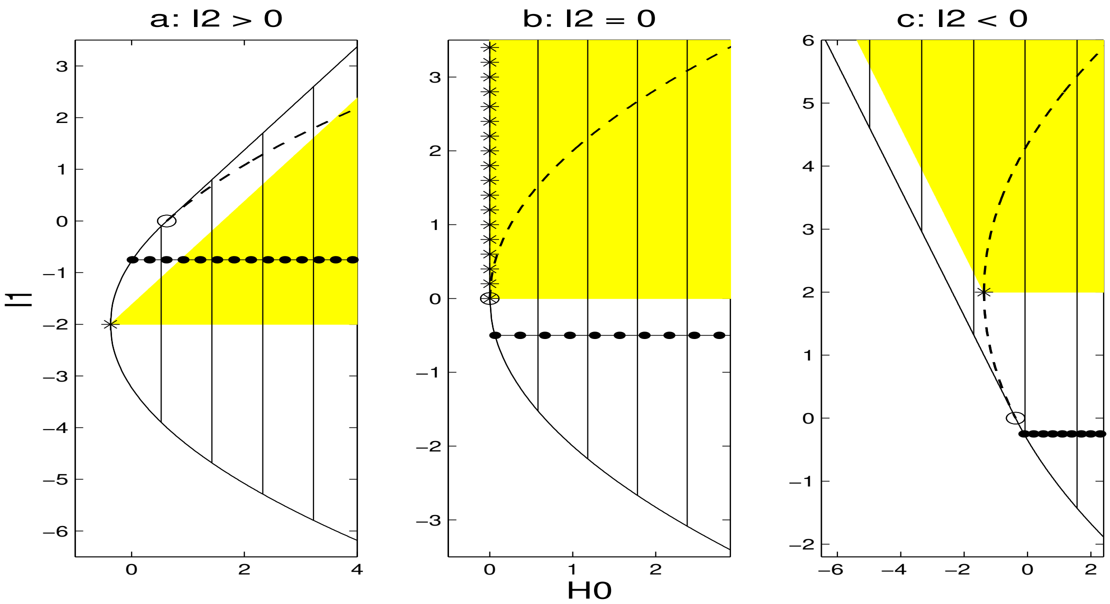

Figure 6: Slices of the energy-actions bifurcation diagram for $\alpha_1 = 0$. $\alpha_1 = 0, \alpha_2 = 1, \alpha_3 = 2$. **a:** $I_2 = 0.5$; **b:** $I_2 = 0$; **c:** $I_2 = -0.5$

Namely, when the elliptic equilibria surface corresponding to $(x, y) = (\pm\sqrt{I_1}, 0)$ folds in the I_1 direction. Equation (5) holds for:

$$I_{2_{ell-res}}(I_1) = -\frac{\alpha_1}{\alpha_3} I_1, \tag{6}$$

for positive values of I_1 and corresponds to two $(1, 0)$ 1-resonant 2-tori which are normally elliptic. It follows that when $\frac{\alpha_1}{\alpha_3}$ is positive (negative) the bounding equilibria surface folds to the right (left), hence $H_{0_{ell-\min}}$ corresponds to the minimal (maximal) energy value for which the equilibria curves corresponding to $(x, y) = (\pm\sqrt{I_1}, 0)$ are defined, see figure 5:c (figure 7:a). Note that for non-positive α_1 the parabolic resonance scenario results in a fundamental change of the energy surface properties - from being locally bounded in I_1 direction near the resonance for, say $I_2 > 0$ to being locally unbounded there for $I_2 \leq 0$.

When $\dot{\theta}_2$ vanishes a $(0, 0, 1)$ resonance occurs. This is indicated in figures 1 and 9 by a surface of dotted lines and in figures 5 - 8 by dotted lines. In the integrable system (2), $\dot{\theta}_2$ vanishes identically when:

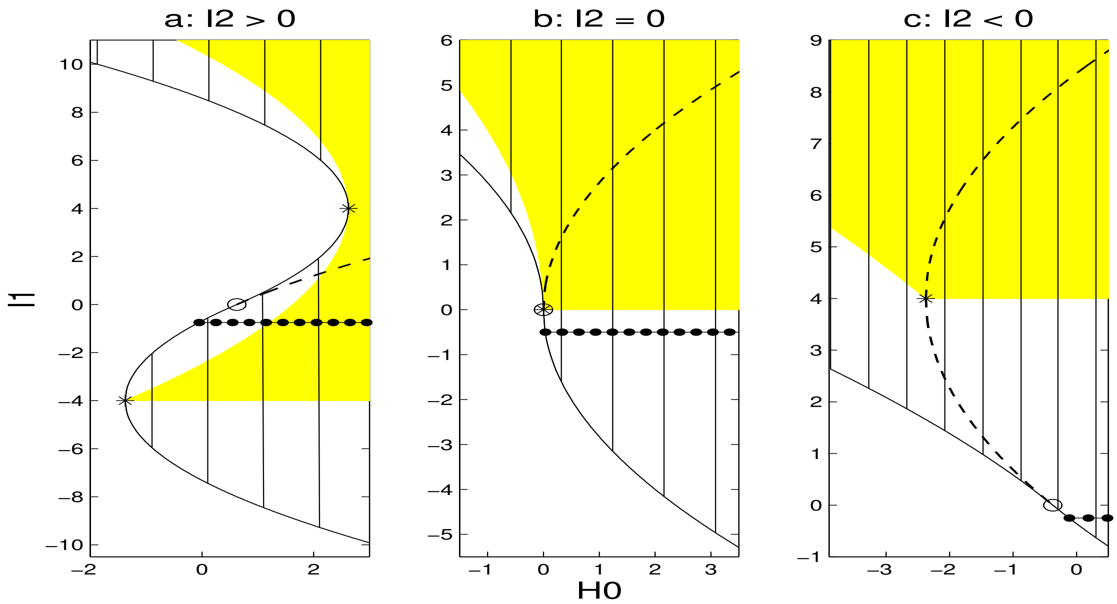

Figure 7: Slices of the energy-actions bifurcation diagram for $\alpha_1 < 0$. $\alpha_1 = -0.25, \alpha_2 = 1, \alpha_3 = 2$. **a:** $I_2 = 0.5$; **b:** $I_2 = 0$; **c:** $I_2 = -0.5$

$$\dot{\theta}_2 = \frac{\partial H_0}{\partial I_2} = 0, \tag{7}$$

Namely when the energy surface has a fold in the I_2 direction. Equation (7) holds for:

$$I_{2_{res2}}(I_1) = -\alpha_2 - \alpha_3 I_1. \tag{8}$$

In figure 8:b the dotted line, which corresponds in this figure to $I_2 = I_{2_{res2}}(0) = -\alpha_2$, intersects the 'o', which marks the parabolic torus. In section 2.2, the corresponding 1-PR that occurs in the near integrable system is referred to as 1-PR in I_2 direction. We emphasize that in figures 1 and 9 the grey volume corresponds to the existence of instantaneous zeroes of $\dot{\theta}_1$, which possibly contain a resonance surface on which $\omega_2 = 0$. The two dimensional dark surfaces correspond to real resonance in the I_2 direction, namely $\omega_3 = 0$.

We see that these diagrams enable one to summarize the global structure of the integrable systems for all energy levels. It is seen that critical energy levels may be easily identified (e.g. in figure 8a,b,c there exist (slices of) energy surfaces (in I_2) for which parabolic resonances exist - see figures 10,

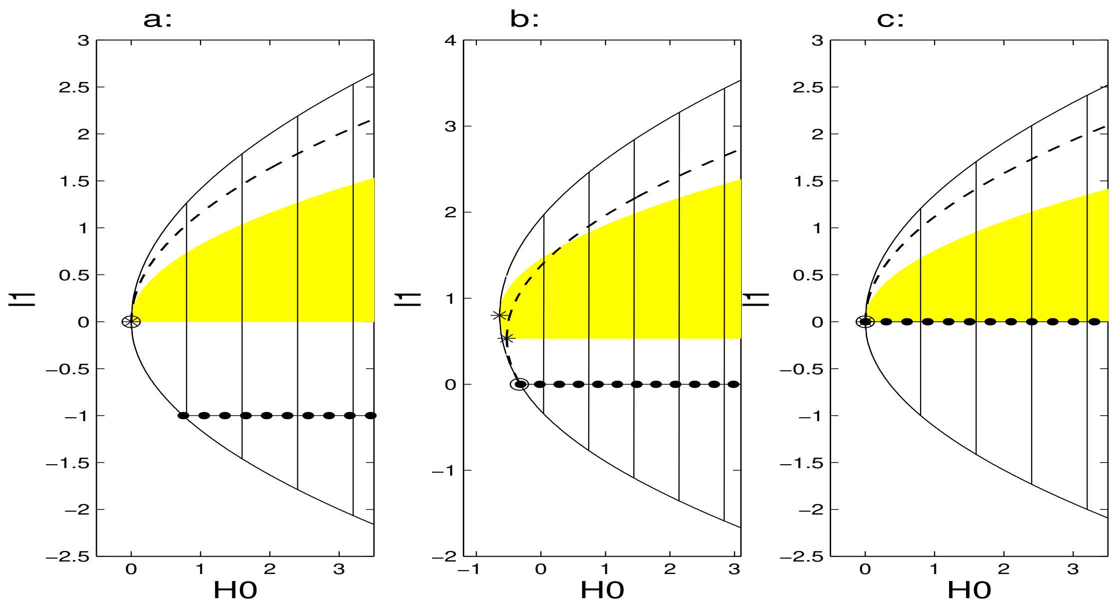

Figure 8: Slices of the energy-actions bifurcation diagrams at parabolic resonances with $\alpha_1 > 0$.
$\alpha_1 = 1.05, \alpha_3 = 2$. **a:** $I_2 = 0, \alpha_2 = 1$: parabolic 1-resonance in the direction of I_1 ($\{(1,0,0),(0,1,0)\}$ resonance); **b:** $I_2 = -\alpha_2 = -1$: parabolic 1-resonance in the direction of I_2 ($\{(1,0,0),(0,0,1)\}$ resonance); **c:** $I_2 = \alpha_2 = 0$: parabolic 2-resonance ($\{(1,0,0),(0,1,0),(0,0,1)\}$ resonance).

12 and 14 for the corresponding dynamics in the near integrable system), and bifurcations induced by external parameters result in qualitative changes in these diagrams (e.g. compare 5 - 7). Furthermore, under small perturbation the Hamiltonian is preserved and the sources of instability for any given energy level are explicitly visible in the diagram.

We are now in position to identify possible sources of substantial instabilities in the near integrable system.

When $\dot{\theta}_1$ and $\dot{\theta}_2$ of the integrable system vanish simultaneously on an invariant 2-torus, two independent resonance conditions are met, and a 2-resonance occur in the near integrable system. When the parameter $\alpha_2 = 0$, this event occurs at O_{xyI}, and a 2-PR takes place in the near integrable system. Appearance of a normally parabolic 2-resonant torus on a certain energy surface may be seen in figure 8:c. In this figure an energy-action

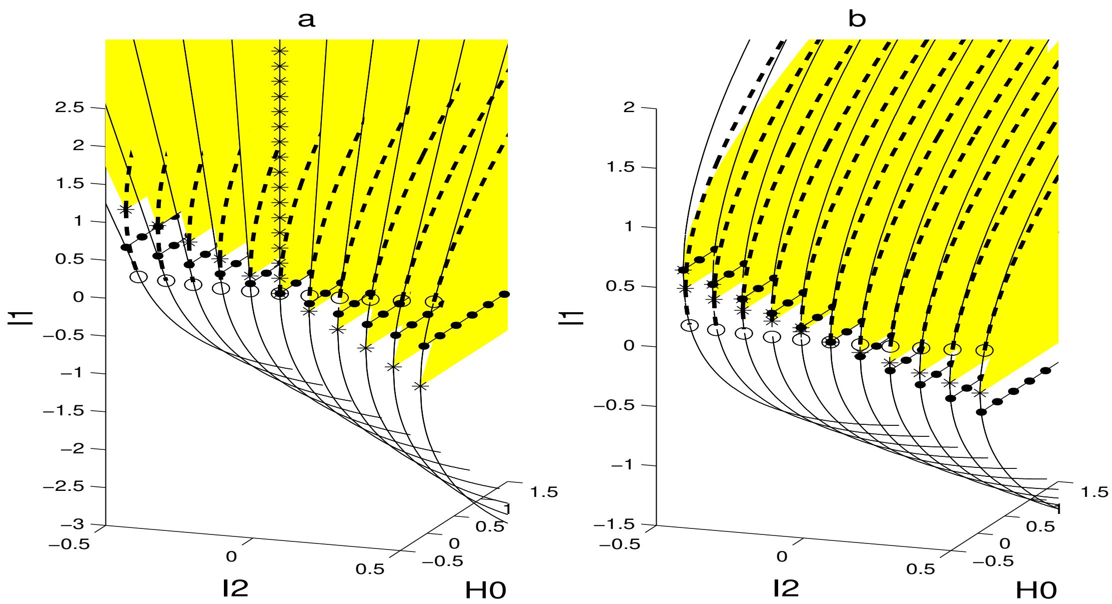

Figure 9: Two types of flat parabolic resonances.
$\alpha_2 = 0, \alpha_3 = 1$. **a:** $\alpha_1 = 0, I_2 = -0.5 : 0.05 : 0.5$; **b:** $\alpha_1 = {\alpha_3}^2 = 1, I_2 = -0.5 : 0.05 : 0.5$

bifurcation diagram in which equations (4) and (8) hold simultaneously at the parabolic torus is presented. In this case the integrable system exhibits a triple resonance, and the near integrable system exhibit large instabilities, as described in section 2.2.

When $\alpha_1 = 0$, it follows from equation (6) that $I_{2_{ell-res}}(I_1) \equiv 0$ for any positive value of I_1. Hence, a whole family of elliptic 1-resonant tori (asterisks in 9:a), together with the *parabolic* resonant torus at the origin, reside on the same energy surface $H_0 = 0$. Furthermore, this energy surface is unbounded in the positive direction of I_1 (figures 6:b and 9:a). This scenario induces a flat 1-PR in the near-integrable case, leading to order one instabilities in I_1 of nearby initial conditions. Such large instabilities in I_1 are possible as the energy surface is unbounded in its positive direction. When $\alpha_1 > 0$ but small, the energy surface is large in I_1, but still bounded, and perturbed orbits are seen to reach the boundaries of such energy surfaces (see for example figure 11).

When $\alpha_1 = \alpha_3^2$ and $\alpha_2 = 0$, from equations (6) and (8) it follows that $I_{2_{ell-res}}(I_1) = I_{2_{res2}}(I_1) = -\alpha_3 I_1$ for any positive value of I_1. Hence, for these parameters values, a whole family of 2-resonant elliptic tori (for positive values of I_1) together with a *parabolic* 2-resonant torus (corresponds to vanishing of I_1) reside on the same unbounded energy surface of the integrable system along the line $I_2 = -\alpha_3 I_1$, see figure 9:b. Indeed, a flat 2-PR occurs in the perturbed system on near by energy surfaces, and very large instabilities are observed in numerical experiments in the positive direction of I_1 and in the negative direction of I_2.

The degeneracy in the integrable system which cause the energy surfaces to be unbounded in the I_1 direction, for certain values of I_2 and of the parameters, is the appearance of a whole family of resonant tori of mixed stability types (hence containing a parabolic resonant torus) on the same energy surface. This happens when all the terms in I_1 vanishes in $\dot{\theta}_1$ for a whole range of the action I_1, which is responsible for the stability type of the invariant 2-tori. Since we consider in (1) only terms up to quadratic order in I_1, we can arrange such scenarios by varying one or two parameters. In figures 6b and 9b we present such situations, where a line of asterisks is seen to cover a whole line of I_1 values. In the generic case this situation is of infinite co-dimension; tangential PRs, which are the first approximation to the flat PRs are a low co-dimension (one or two) phenomena (see [11]).

In section 2.2 we describe the corresponding scenarios in the near integrable system.

2.2 The near integrable system

For 3 d.o.f. near integrable systems there are 3 types of parabolic resonance:

Case 1: Parabolic 1-resonance in I_1 direction ($\dot{\theta}_1 = 0$ in the integrable system, figure 8:a).

Case 2: Parabolic 1-resonance in I_2 direction ($\dot{\theta}_2 = 0$ in the integrable system, figure 8:b).

Case 3: Parabolic 2-resonance ($\dot{\theta}_1 = \dot{\theta}_2 = 0$ in the integrable system, figure 8:c).

In cases 1 and 2 the parabolic 2-torus is a torus of closed invariant periodic orbits, and in the third case it is a parabolic 2-torus of fixed points.

We examine numerically the effect of small Hamiltonian perturbation on each of the above cases. The figures and descriptions below correspond to

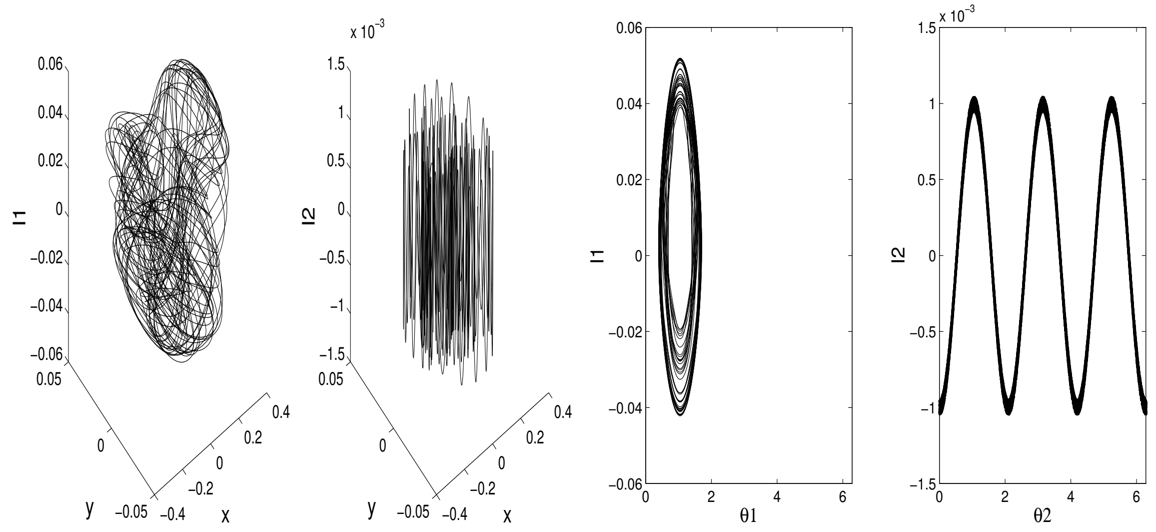

Figure 10: A parabolic 1-resonance in I_1 direction.
Initial conditions and parameters: $(x, y, \theta_1, I_1, \theta_2, I_2) = (0.2, 0, 1.57, 0, 1.57, 0)$, $\alpha_1 = 1, \alpha_2 = 1, \alpha_3 = 1$, $\varepsilon_1 = \varepsilon_2 = 1e-3$, $H_0 \approx 4E-4$, $t = 5000$. Notice the different scales of I_1 and I_2.

the following perturbation:

$$H_1 = \varepsilon_1(1 - \frac{x^2}{2})\cos(k_1\theta_1) + \varepsilon_2\cos(k_2\theta_2), \qquad \varepsilon = \varepsilon_1 = \varepsilon_2. \tag{9}$$

Other forms of Hamiltonian perturbations seems to produce qualitatively the same results.

Case 1 : Figure 10 presents the apparent chaotic behavior of the orbit, and the trapping in the parabolic resonance zone in the (x, y, I_1) space and in the (θ_1, I_1) plane, together with the small oscillations of the orbit in the I_2 direction. Figure 11 presents again a 1-PR in I_1 direction, with smaller α_1 value ($\alpha_1 = 0.3$). It demonstrates that the instabilities in I_1 are much stronger as α_1 is decreased. We propose that the source for this instability is the geometrical change of the unperturbed energy surface - for a given energy value near the PR, as α_1 is decreased the range of I_1 increases, approaching the unbounded range as $\alpha_1 \to 0$, where a flat PR occurs (see section 2.1). We numerically observe that it becomes significant when $\alpha_1 < 0.5$. We stress

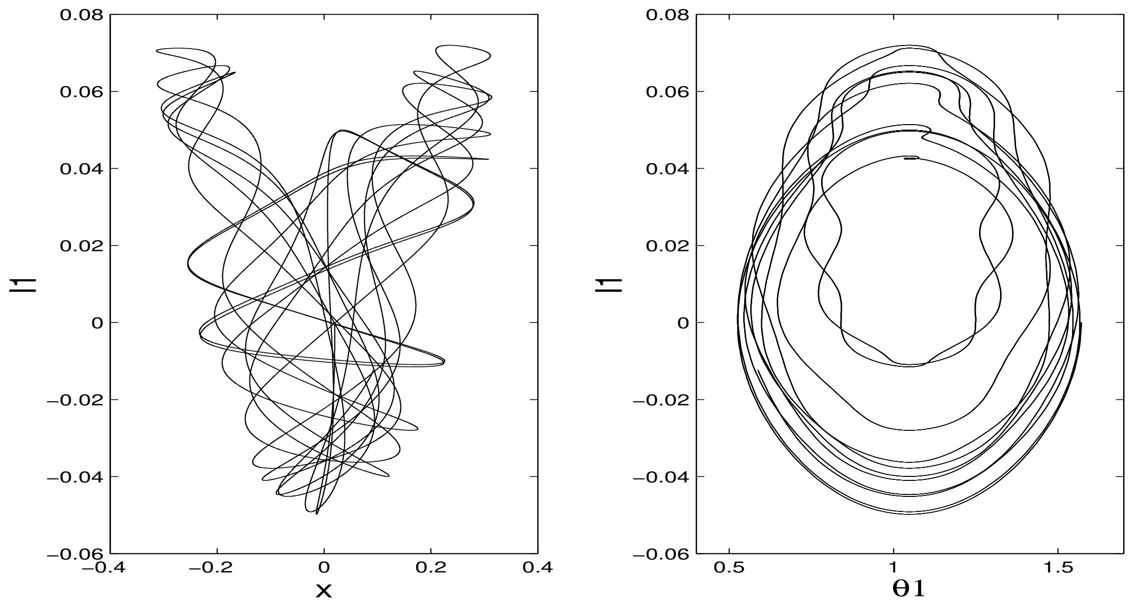

Figure 11: A parabolic 1-resonance in I_1 direction. Initial conditions and parameters: $(x, y, \theta_1, I_1, \theta_2, I_2) = (0.2, 0, 1.57, 0, 1.57, 0)$, $\alpha_1 = 0.3, \alpha_2 = 1, \alpha_3 = 1$, $\varepsilon_1 = \varepsilon_2 = 1e - 3$, $H_0 \approx 4E - 4$, $t = 1000$.

that in all simulations of this case the perturbed orbit appears to reach the boundaries of its energy surface in I_1, which implies that the 1-PR in I_1 direction induces the strongest possible instabilities in I_1, see figure 17 for illustration. Furthermore, the motion in I_1 appears to be chaotic, and the perturbed orbits exhibit a very similar structure to the 2 d.o.f. orbits of [15].

Case 2 : Figure 12 demonstrates that both actions exhibit quasi-periodic motion (see zoom in on the right plot). Figure 13 presents a projection to the (x, y) plane of the orbits of cases 1 and 2. While the 1-PR in I_1 direction exhibits a parabolic resonance chaos as in the 2 d.o.f. case, the 1-PR in I_2 direction fills in a complicated structure. Such complicated structures are observed for a range of initial conditions and parameters near 1-PR in I_2 direction. The different roles of the actions in the system is now apparent. As this separation of roles of the actions is achieved by a simplectic change of variables on the integrable Hamiltonian, the two scenarios are expected to appear in any general near integrable Hamiltonian exhibiting parabolic resonances.

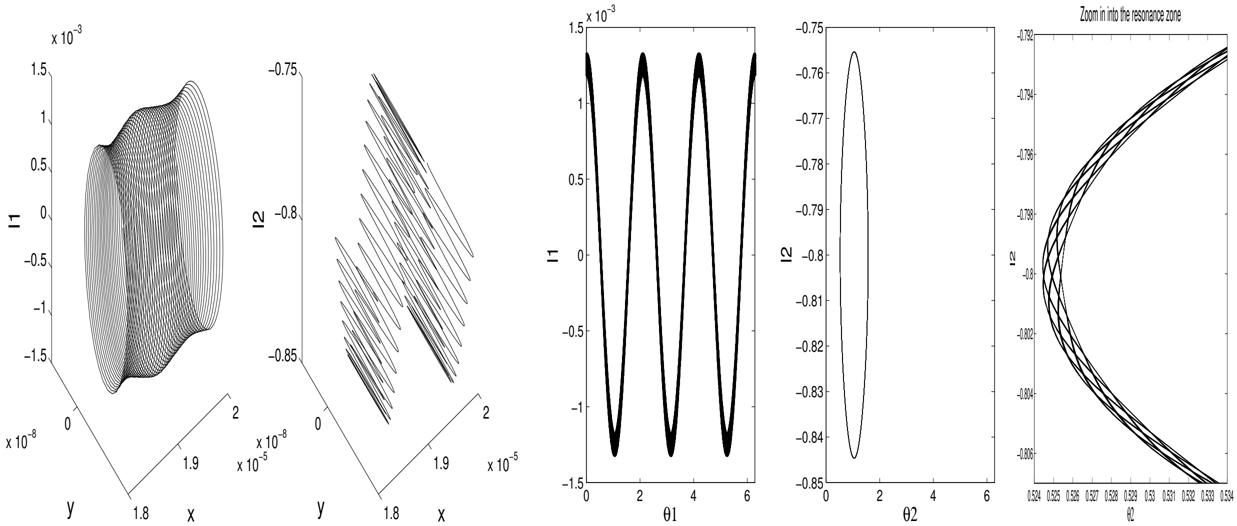

Figure 12: A parabolic 1-resonance in I_2 direction. Initial conditions and parameters: $(x, y, \theta_1, I_1, \theta_2, I_2) = (2E-5, 0, 1.57, 0, 1.57, -0.8)$, $\alpha_1 = 1, \alpha_2 = 0.8, \alpha_3 = 1$, $\varepsilon_1 = \varepsilon_2 = 1e-3$, $H_0 \approx 4E-4$. Left two plots: $t = 300$, Right plots: $t = 5000$. Notice the different scales of I_1 and I_2.

Case 3 : Figure 14 demonstrates that the resonance zones and large instabilities are created in both actions. Notice that the *system is non-degenerate*. This behavior should be contrasted with the 2 d.o.f. case, in which such instabilities in the action variable are possible only in degenerate cases, when the necessary conditions for KAM theory fail. We prove in [11] that cases 1 and 2 are persistent in 3 d.o.f. near integrable Hamiltonian systems without the use of external parameters (where the actions serve as internal parameters), and that case 3 is persistent in a one parameter family of near integrable 3 d.o.f. Hamiltonian systems.

The single case of degenerate (flat) parabolic resonance in the 2 d.o.f. system has several generalizations in the 3 d.o.f. setting. One set of generalizations is simply attained by setting $\alpha_1 = 0$, in addition to the conditions appearing in each case. Another generalization is attained by setting $\alpha_2 = 0$, and $\alpha_1 = \alpha_3^2$, see end of section 2.1. The numerical experiments of case

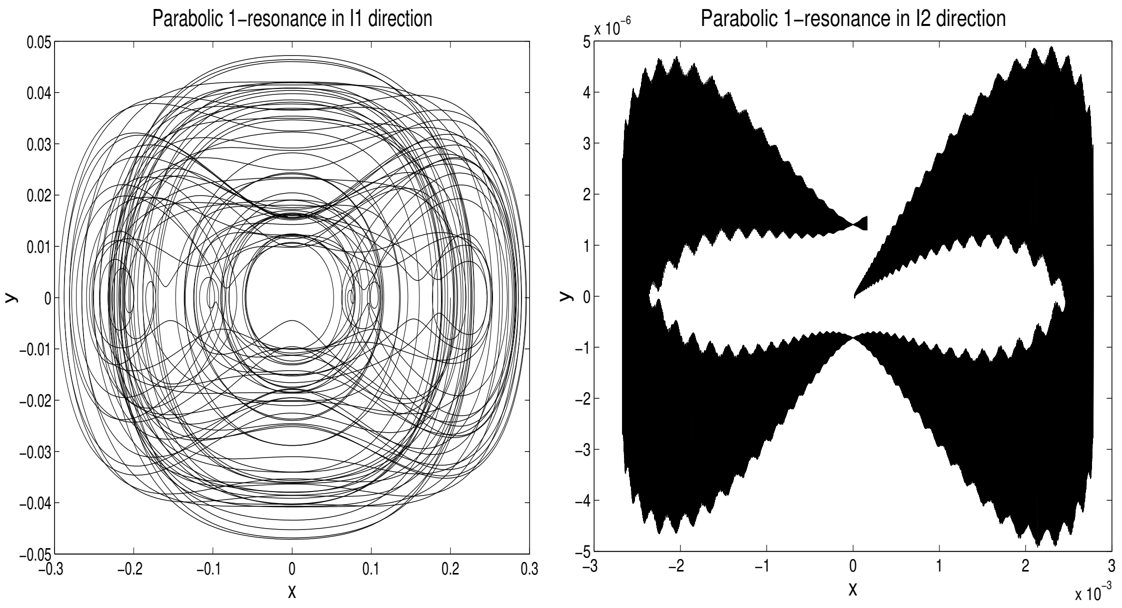

Figure 13: Parabolic 1-resonances projected on the (x, y) plane.
Initial condition and parameters: as in figures 10 with $t = 5000$ and 12 with $t = 8700$, respectively.

1 with $\alpha_1 < 0.5$ demonstrated that the behavior in the near-flat case[7] is similar to the one observed in the 2 d.o.f. model. Yet, in the flat PR case, the order one instabilities in I_1 direction develop *slower* than in the 2 d.o.f. case, probably due to the small oscillations in the I_2 direction, see figures 15 and 16 for comparison. Figure 17 demonstrates that orbits exhibiting near flat PR cover the corresponding unperturbed energy surface, and repeatedly reach the boundaries (in I_1) of the perturbed energy surface to which they belong, while repeatedly passing through the parabolic resonance zone. In the right plot of this figure we present the orbit (in light gray) covering the corresponding unperturbed energy surface (in black), which is presented separately on the left plot. Two other cases of near flat parabolic resonances demonstrating order one instabilities in all phase space directions are observed. Such perturbed orbits have a complicated structure and they wander through successive resonance zones that are created in both actions. Fig-

[7]Recall, here the flat PR has $\alpha_1 = 0$, whereas near-flat PR has $\alpha_1 \ll 1$ (and in practice $\alpha_1 < 0.5$).

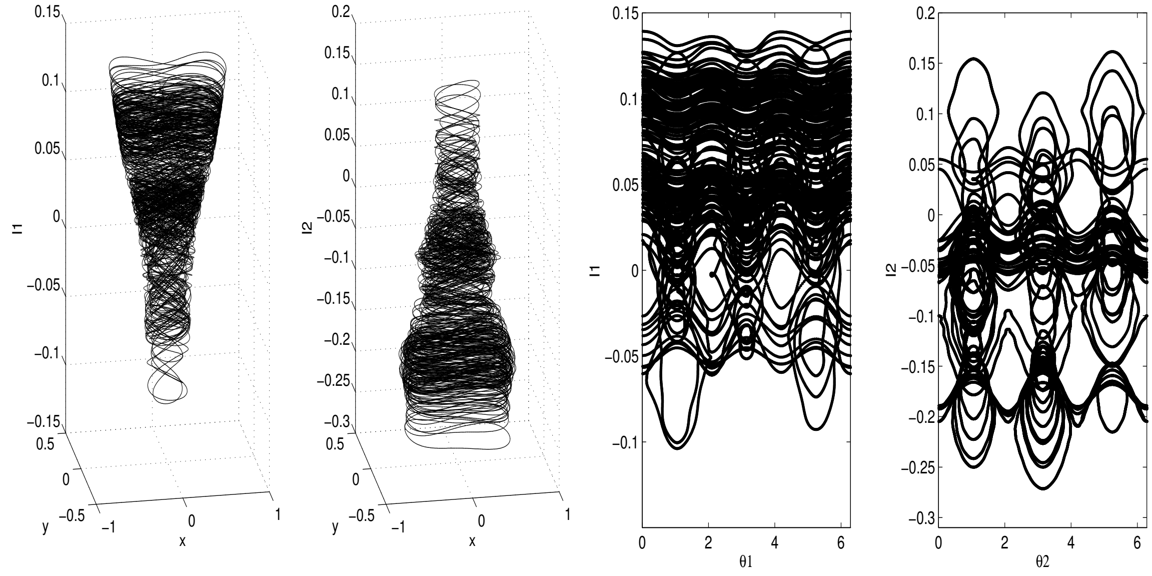

Figure 14: A parabolic 2-resonance.
Initial conditions and parameters: $(x, y, \theta_1, I_1, \theta_2, I_2) = (0.2, 0, 1.57, 0, 1.57, 0)$, $\alpha_1 = 1.1, \alpha_2 = 0, \alpha_3 = 2$, $\varepsilon_1 = \varepsilon_2 = 1e-3$, $H_0 \approx 4E-4$, $t = 5,000$.

ures 18, 19 and 20 present two types of flat 2-PR. In the first case (figure 18, $\alpha_1 = \alpha_2 = 0$), a parabolic resonant torus of fixed point and a family of elliptic tori of *periodic orbits* reside on the same unperturbed energy surface, whereas in the second case a parabolic resonant torus of fixed point and a family of elliptic tori of *fixed points* reside on the same unperturbed energy surface (figures 19 and 20, $\alpha_2 = 0$, and $\alpha_1 = \alpha_3^2$). In figure 19 the instabilities exhibited by the perturbed orbit in the (x, y, I_1) and (x, y, I_2) spaces are shown in the top plots, and the corresponding slices of the unperturbed energy surfaces are shown in the bottom plots. It is seen that although these slices of the unperturbed energy surfaces are small the instabilities are large. Indeed, since the instabilities occur in both actions, slices attained by fixing one of them do not reflect the unboundedness of the energy surface in the $I_2 = -I_1$ direction, the direction along which the instabilities develop (see figure 9). Figure 20 presents the projection of the same perturbed orbit on the (θ_1, I_1) and (θ_2, I_2) planes. In this figure the spring like structure of the orbit which passes through the successive multi-resonance zones is shown.

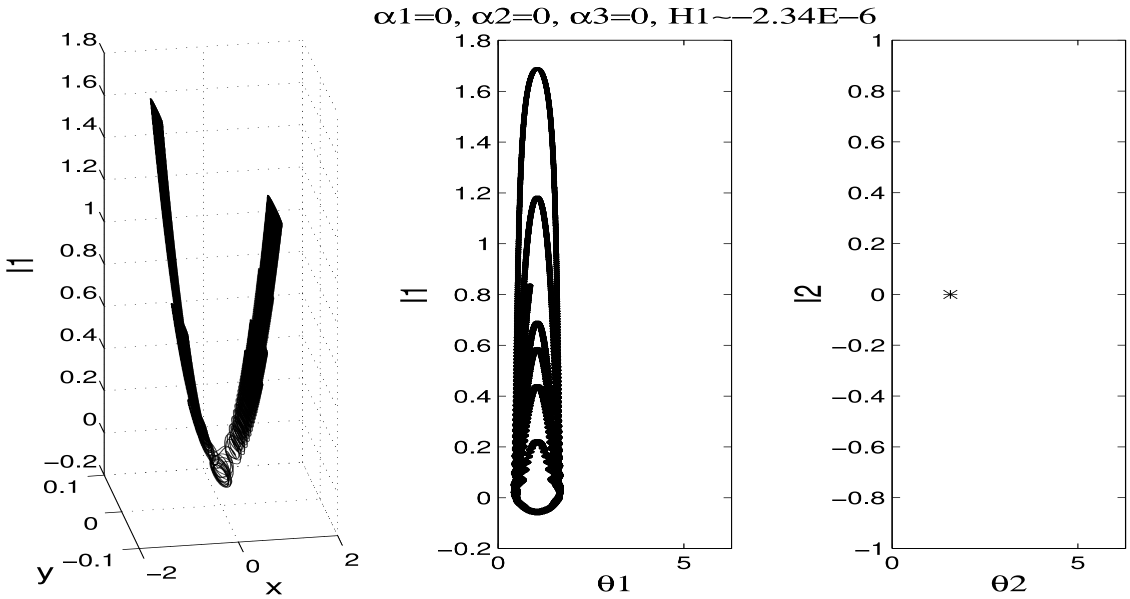

Figure 15: A flat parabolic resonance in a 2 d.o.f. system.
Initial conditions and parameters: $(x, y, \theta_1, I_1, \theta_2, I_2) = (0.2, 0, 1.57, 0, 1.57, 0)$, $\alpha_1 = 0, \alpha_2 = 0, \alpha_3 = 0$, $\varepsilon_1 = 1e - 3, \varepsilon_2 = 0$, $H_0 \approx 4E - 4$, $t = 8,000$.

The most important feature of the instabilities associated with the flat, near flat and tangential parabolic resonances is that they develop on relatively short time scales. For example, in the parabolic 2-resonance case large instabilities occur, but their development is relatively slow, obeying one time scale, while in the cases of the flat parabolic resonance, two time scales (slow and fast) coexist. On the slow time scale, the orbit is trapped in a resonance zone, and on the fast time scale it makes far trips sliding through successive resonance zones. In the tangential 2-resonance case, (a co-dimension 2 phenomenon [11]) these fast trips may occur in all phase space directions simultaneously.

It still remains to calculate analytically the rate of instability created in each of the cases of parabolic and tangential parabolic resonance.

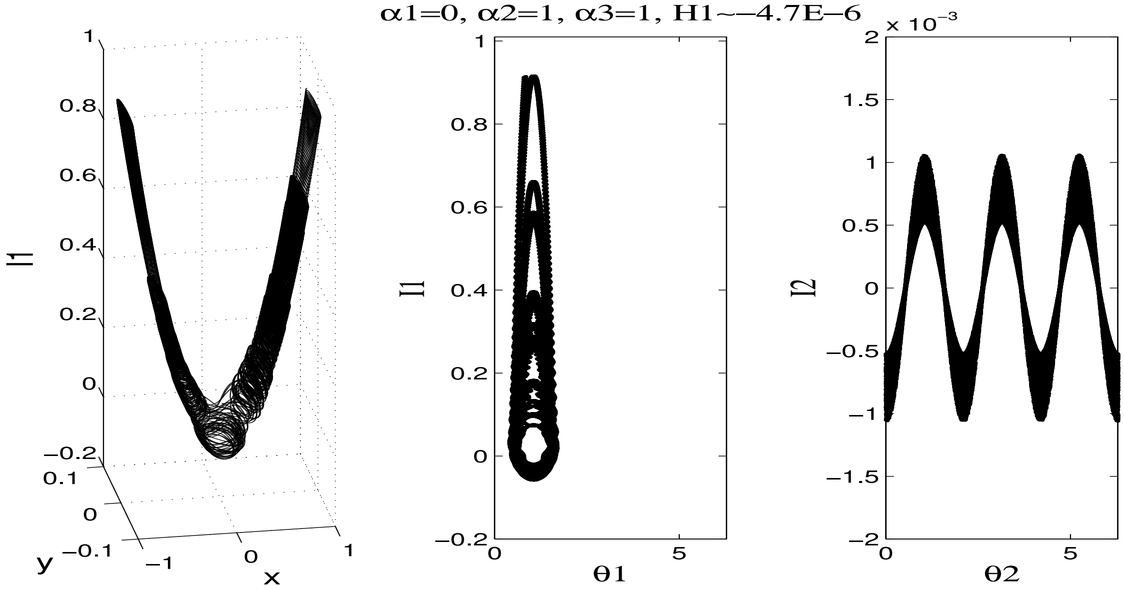

Figure 16: A flat parabolic 1-resonance in a 3 d.o.f. system.
Initial conditions and parameters: $(x, y, \theta_1, I_1, \theta_2, I_2) = (0.2, 0, 1.57, 0, 1.57, 0)$, $\alpha_1 = 0, \alpha_2 = 1, \alpha_3 = 1$, $\varepsilon_1 = \varepsilon_2 = 1e - 3$, $H_0 \approx 4E - 4$, $t = 8,000$.

3 The motion of weather balloons - a model.

The Hamiltonian (10) corresponds to a 3 d.o.f. model describing the motion of particles (weather balloons) on a rotating sphere (geopotential surfaces of the earth atmosphere) which are subject to a conservative force (traveling wave pressure term) which breaks the angular symmetry. Here we add to the atmospheric model studied in [16] a third degree of freedom, which describes the small altitude oscillations of the weather balloons. For the 2 d.o.f. case (taking $\varepsilon_2 = 0, D_2 = 0$ in (10)) the global phase space structure of the unperturbed system has been described by the shaded energy momentum bifurcation diagrams (bifurcation diagrams in the space of constants of motion). In [15, 17] the phenomena of PR was discovered, has been shown to exist in this model, and it has been demonstrated that this PR is a source of strong, yet rare phase space instability, with qualitative agreement to the observations of motion of weather balloons in field experiments. Here, this model serves us as a test case application for our findings for the phenomeno-

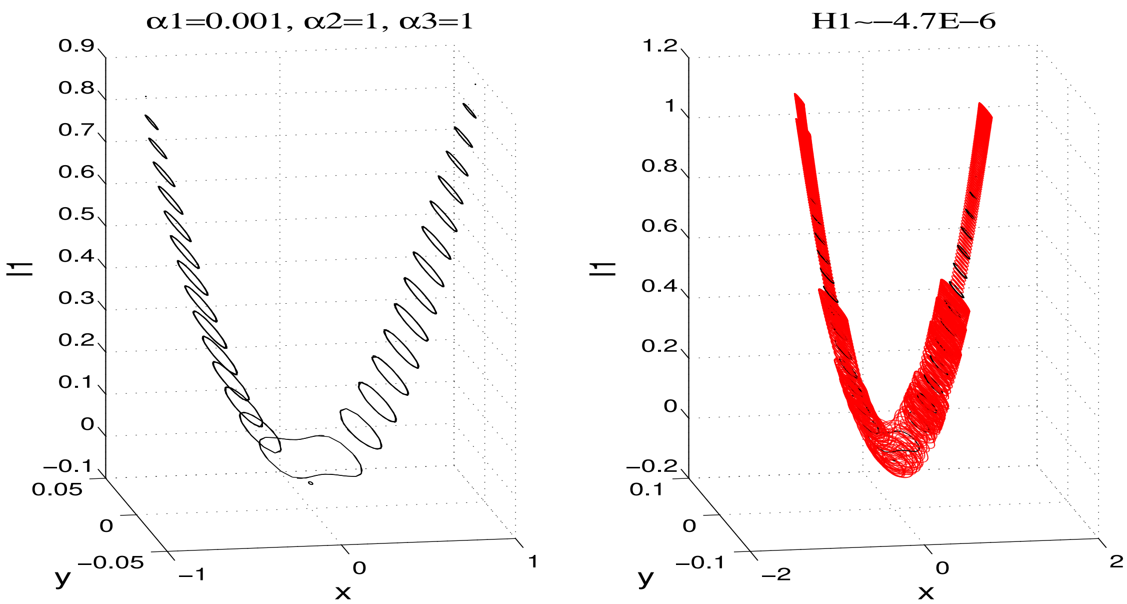

Figure 17: A near flat parabolic 1-resonance in a 3 d.o.f. system, and the corresponding unperturbed energy surface. Initial conditions and parameters: $(x, y, \theta_1, I_1, \theta_2, I_2) = (0.2, 0, 1.57, 0, 1.57, 0)$, $\alpha_1 = 0.001, \alpha_2 = 1, \alpha_3 = 1$, $\varepsilon_1 = \varepsilon_2 = 1e-3$, $H_0 \approx 4E-4$, $t = 8,000$.

logical model. Indeed, all types of behavior which is described above for PR and flat/tangential PR that are observed for the phenomenological model are observed for this atmospheric model as well. For example, see figure 21, where an orbit, exhibiting a near flat 2-PR projected on the (ϕ, v, D_1) (left plot) and (ϕ, v, D_2) (right plot) spaces are shown. Compare this figure with figure 18 of the phenomenological model. This near flat 2-PR, which results in instabilities in all phase space directions simultaneously, is a 3 d.o.f. phenomenon.

To describe the weather balloon motion on the rotating sphere with a given traveling pressure wave velocity c, we use normalized, relative spherical coordinate system; let ϕ be the latitude on the sphere and v its conjugate northward velocity, Λ_1 the longitude in the traveling wave frame and D_1 its conjugate angular momentum. Finally, let Λ_2 denote the normalized vertical oscillation amplitude and D_2 its conjugate momenta. The new 3

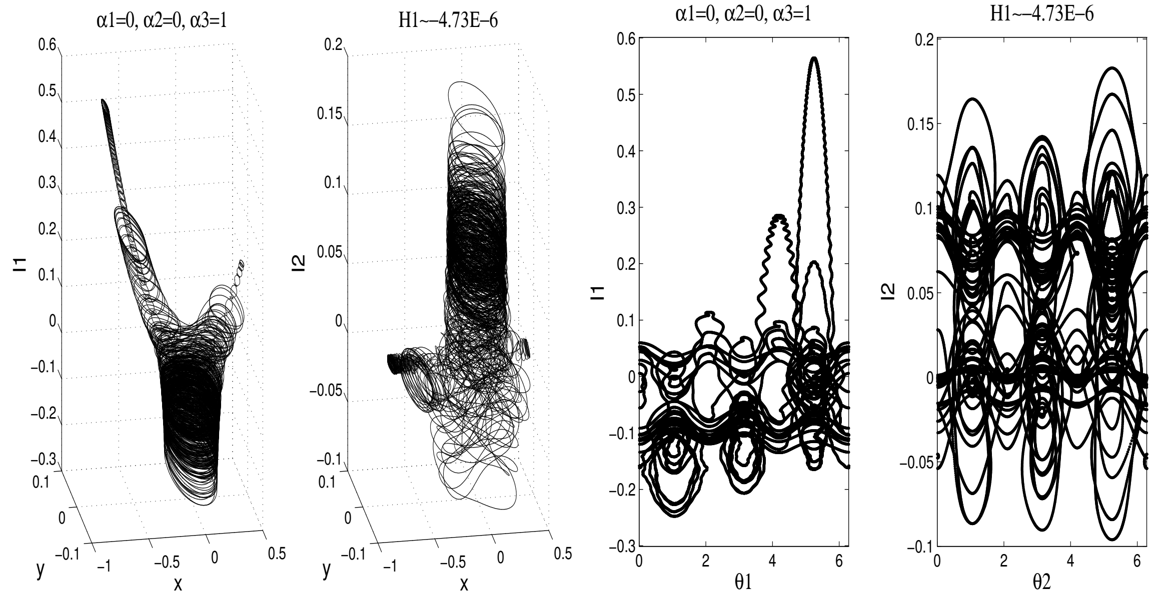

Figure 18: A flat parabolic 2-resonance. Initial conditions and parameters: $(x, y, \theta_1, I_1, \theta_2, I_2) = (0.2, 0, 1.57, 0, 1.57, 0)$, $\alpha_1 = 0, \alpha_2 = 0, \alpha_3 = 1$, $\varepsilon_1 = \varepsilon_2 = 1e-3$, $H_0 \approx 4E-4$, $t = 8,000$.

d.o.f. Hamiltonian is given by:

$$\begin{aligned} H(\phi, v, \Lambda, D; \mu, k, \varepsilon) &= \frac{v^2}{2} + \frac{1}{8}\left(\frac{2D_1}{\cos(\phi)} - \cos(\phi)\right)^2 + \frac{D_2^2}{2} - cD_1 + \\ &+ aD_2\left(D_1 - \frac{1}{2}\right) + bD_2 + B(\phi; \beta) + \\ &+ A(\phi)(\varepsilon_1 \sin(k_1\Lambda_1) + \varepsilon_2 \sin(k_2\Lambda_2)) \\ &= H_0(\phi, v, D; \mu) + H_1(\phi, v, \Lambda, D; \mu, k, \varepsilon), \\ (\phi, v, \Lambda, D) \in U \subseteq \mathbb{R}^2 \times \mathbb{T}^2 \times \mathbb{R}^2, &\quad k \in \mathbb{Z}, \beta, \varepsilon \in \mathbb{R}^2, |\varepsilon| \ll 1, \end{aligned} \tag{10}$$

where $\mu = (a, b, c, k_1, k_2, \beta)$ with $a, b, c, \beta \in \mathbb{R}$, $k_1, k_2 \in \mathbb{Z}$, $\varepsilon_1, \varepsilon_2 \ll 1$. $A(\phi)$ and $B(\phi)$ represent the latitude-dependent amplitudes of the traveling pressure wave and the constant pressure term, respectively. In our numerical experiments they are taken to be of the form:

$$\begin{aligned} A(\phi) = \cos(\phi), \quad B(\phi; \beta) = \beta \tanh\left(\frac{\phi^2 - \phi_0^2}{\alpha}\right), \\ \phi_0 = 30^o \approx 0.5236, \quad \alpha = 0.05, \quad \beta = -0.001 \end{aligned} \tag{11}$$

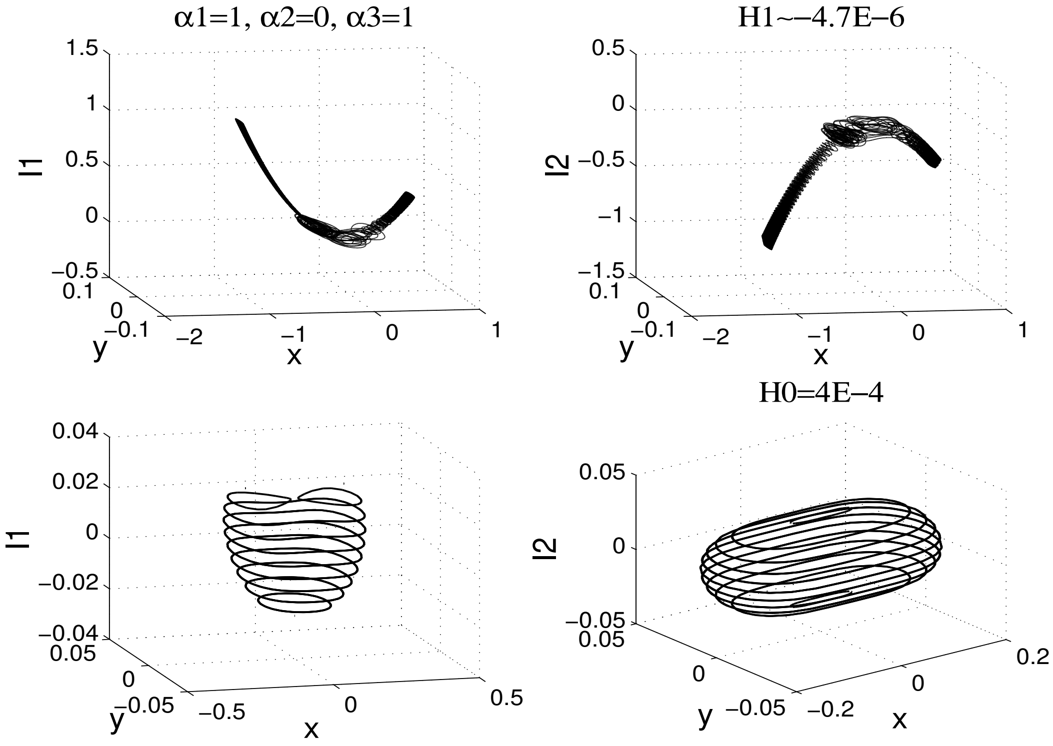

Figure 19: A flat parabolic 2-resonance.
An orbit and the corresponding unperturbed energy surface are projected on the (x, y, I_1) and (x, y, I_2) spaces.
Initial conditions and parameters: $(x, y, \theta_1, I_1, \theta_2, I_2) = (0.2, 0, 1.57, 0, 1.57, 0)$, $\alpha_1 = 1, \alpha_2 = 0, \alpha_3 = 1$, $\varepsilon_1 = \varepsilon_2 = 1e-3$, $H_0 \approx 4E-4$, $t = 8,000$.

Namely $A(\phi)$ is simply the first symmetric harmonic and $B(\phi)$ represents a steady pressure term that is monotonically decreasing pole-ward, allowing strong zonal jets to appear near ϕ_0. The numerical values appearing in (11) correspond to rough estimates of physical relevant parameter values.

In the 2 d.o.f. case (the Hamiltonian (10), with $\varepsilon_2 = 0, D_2 = 0$) a parabolic resonance occurs for $D_1 = 0.5$, $c = 0$, and a flat (degenerate) parabolic resonance if in addition $B(\phi) = 0$ (the physical relevant case is $|B(\phi)| \ll 1$, hence it corresponds to a nearly flat parabolic resonance). These parabolic resonances correspond to two simultaneous phenomena - the change in the linear stability in latitude direction of particles motion about the

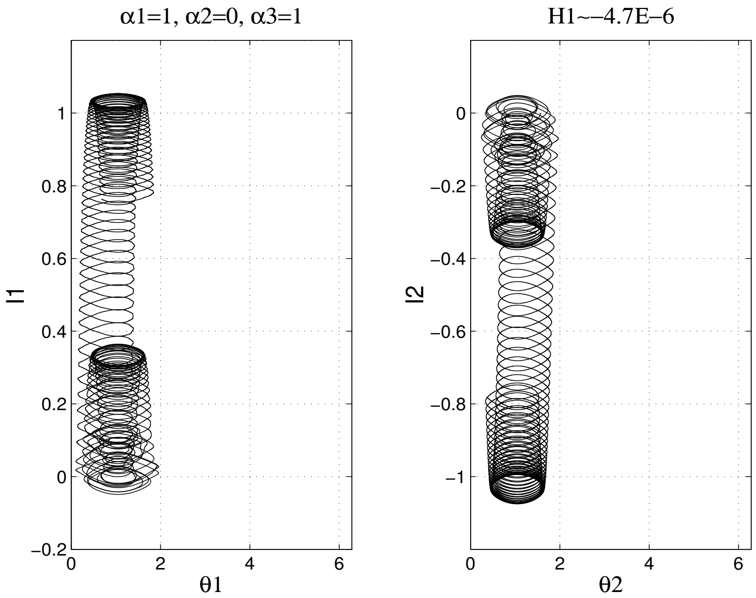

Figure 20: A flat parabolic 2-resonance.
Projections of the orbit on the (θ_1, I_1) and (θ_2, I_2) planes.
Initial conditions and parameters as in figure 19

equator (about $(\phi, v) = (0, 0)$) and the coincidence of the traveling wave speed with the west-ward speed along the equator ($\dot{\Lambda}_1|_{(\phi,v,D_1)=(0,0,0.5)} \equiv 0$).

Adding another degree of freedom to this model, allows PR to occur without external parameter. In (10) the second constant of motion, D_2, replaces the mathematical role of the parameter c of the 2 d.o.f. model. Hence, for any value of c there exist a D_2 value for which a 1-PR occurs for some $D(c)$ $(D(c = 0) = (0.5, 0))$.

4 Persistence of parabolic resonances

We have demonstrated that a simple phenomenological model is rich enough to attain PR of various kinds. The possibility to construct such a model in a straight forward way follows from the *persistence* of PRs in 3 d.o.f. systems. In [11] we prove several theorems regarding the persistence of PRs with various properties in n d.o.f. near integrable Hamiltonian systems. The

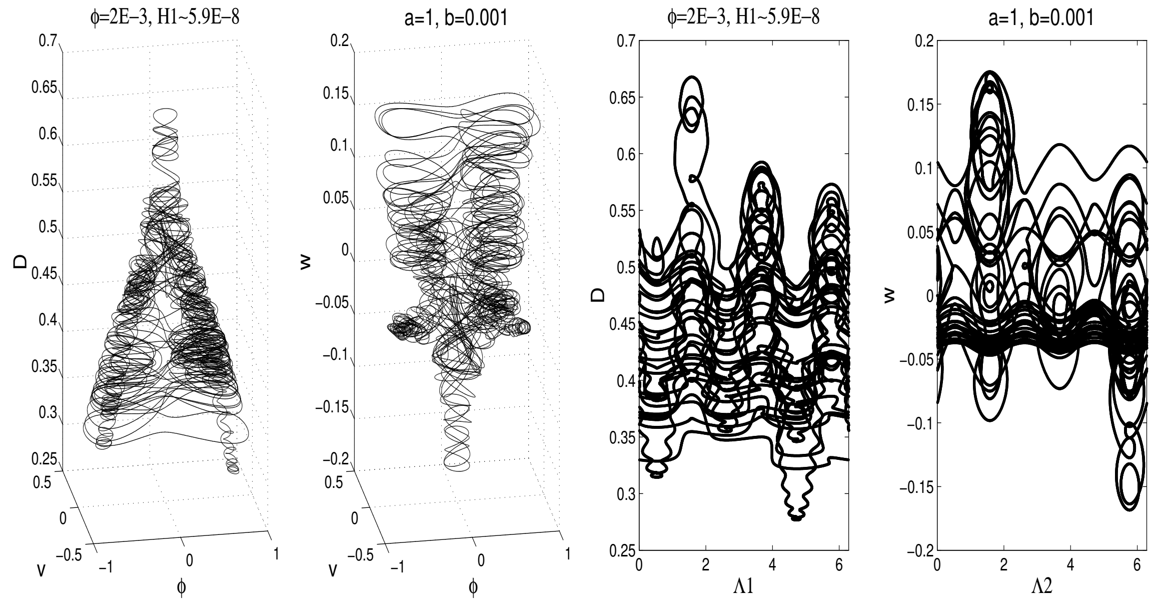

Figure 21: A near flat parabolic 2-resonance in the 3 d.o.f. atmospherical model.
Initial conditions and parameters: $(\phi, v, \Lambda_1, D_1, \Lambda_2, D_2) = (2E-3, 0, 1E-5, 0.5, 1E-5, 0)$, $a = 1, b = 0.001$, $\varepsilon_1 = \varepsilon_2 = 1e-3$, $\beta = -0.001$ $t = 5,000$.

implications of these theorems on the persistence of resonant 2-tori in 3 d.o.f. near integrable systems are listed below:

Theorem 1 *The existence of a normally parabolic* 1*-resonant torus is persistent for smooth near integrable* 3 *d.o.f. Hamiltonian systems, without the use of external parameters. Each such torus consists of a* 1*-dimensional family of circles.*

Corollary 1 *The occurrence of a parabolic* 1*-resonance is persistent in smooth near integrable* 3 *d.o.f. Hamiltonian systems.*

Theorem 2 *The existence of a normally parabolic* 2*-resonant torus (i.e. a normally parabolic* 2*-torus of fixed points) is persistent in a one parameter family of smooth integrable* 3 *d.o.f. Hamiltonian systems.*

Corollary 2 *The occurrence of a parabolic* 2*-resonance is persistent in a one parameter family of smooth near integrable* 3 *d.o.f. Hamiltonian systems.*

Notice that the first corollary deals with cases 1 and 2 of section 2.2 and the second corollary deals with case 3. Indeed, for case 1 and 2 we did not need to fix any parameters in our model, whereas case 3 required fixing one parameter ($\alpha_2 = 0$).

Since our Hamiltonian depends on the actions only up to quadratic terms, we needed to fix only one additional parameter to obtain flat PRs. More generally, fixing one additional parameter results in a tangential PR, which exhibits similar instabilities to the ones obtained in the flat case:

Theorem 3 *The existence of an infinitesimal bundle of normally elliptic and/or normally hyperbolic resonant tori together with a normally parabolic* 1*-resonant (respectively* 2*-resonant) torus, on the same energy surface, is persistent in a one parameter (respectively two parameter) family of smooth integrable* 3 *d.o.f. Hamiltonian systems.*

Corollary 3 *The occurrence of a tangential parabolic* 1*-resonance (respectively* 2*-resonance) is persistent in a one parameter (respectively two parameter) family of smooth near integrable* 3 *d.o.f. Hamiltonian systems.*

5 Summary and Conclusions

By investigating a near-integrable Hamiltonian with an integrable part which is constructed by polynomial expansion in normal co-ordinates, we demonstrated that the phenomena of parabolic resonance (PR) appears in a persistent way in 3 d.o.f. near-integrable systems (this follows from the persistence theorems which are proved in [11]). PRs typically appear in systems in which the integrable part is non-separable. We found that there are two different persistent 1-parabolic resonance scenarios; in one case the action governing the stability of the 2-torus is also involved in the resonance, whereas in the other case one action governs the stability of the two torus and the other action is involved in the resonance. The first case is a direct generalization of the PRs appearing in 2 d.o.f. system, whereas the second, corresponds to a cross product of parabolic bifurcation and a resonance. Numerical simulations suggest that the former gives much stronger instabilities - they are large and occur on a fast time scale. More precisely, the non-bifurcating action oscillates slightly while the action responsible for the PR varies as far as possible - it covers the full range of the unperturbed allowed region of motion (with a fixed second action). The simulations demonstrated that the instabilities near the degenerate flat PR ($\alpha_1 = 0$) leave their mark even on relatively large non-degeneracy parameter ($\alpha_1 < 0.5$). It was proposed that in this case the geometry of the unperturbed energy surfaces determines the extent of the instability - the smaller the non-degeneracy parameter is, the larger the range of the bifurcation action in the nearby energy surfaces and hence the larger is the instability. The other kind of 1-PR does not exhibit strong instabilities, yet produces interesting structures; the actions vary quasi-periodically (the resonant action on a larger scale), and the motion in the normal plane fills a complicated structure.

A 2-torus of fixed points which are normally parabolic, called a 2-PR, appears in a persistent way in a one parameter family of 3 d.o.f. systems. We demonstrated that in this case large (yet slow in comparison to the flat cases) instabilities appear even in the non-degenerate case. We have seen that further degeneracies of this case, corresponding to flat 2-parabolic resonances result in fast and large instabilities in all phase space directions.

The main analytical tool we have used to analyze the system is the construction of bifurcation diagrams in the space of constants of motion. We showed that they give a global and full description of the behavior of the integrable system. Moreover, these bifurcation diagrams are used to deduce which scenarios are expected in the corresponding near integrable system. For example, we saw that the first kind of the 1-PR corresponds to a change of stability at a fold of the bounding surface of the allowed region of motion, and a flat PR corresponds to resonance lines which include the parabolic point and which are perpendicular to the energy axis.

The main idea conveyed here is that PRs are a source of instability which appear inevitably in a large class of higher dimensional systems. Here we have constructed a simple model to demonstrate how strong the influence of such instabilities may become, and in a later work [11] we examine how the mechanisms of instabilities can become more and more degenerate (hence more influential) as the dimensionality of the system grows.

Many issues remain to be addressed in the future. First, a precise estimate (numerical and analytical) of the instability strength needs to be established and compared to other mechanisms of instabilities in 3 d.o.f. systems. Since the motion appears to be recurrent (with long excursions), this requires a good definition of escape. We have made some preliminary progress in this direction. A second natural question is whether the orbits near the various kind of PRs are chaotic. Our numerical investigation suggests that the orbits structure is very different in each of the cases. Perhaps techniques used in the "dynamic bifurcation" literature may be utilized here [10, 12]. A deep open question is the relation of all this to Arnold diffusion or, more precisely, to instability mechanisms in a-priori stable systems. We believe that similar mechanisms arising from resonance interactions exist. A precise calculation is yet to be done.

A Conditions and assumptions for the construction of the phenomenological model

The conditions for an *integrable* 3 d.o.f. Hamiltonian system with a Hamiltonian $H_0 = H_0(x, y, I_1, I_2; \mu)$, and with the simplectic structure:

$$dx_i \wedge dy_i + \sum_{i=1}^{2} d\theta_i \wedge dI_i;\ x, y, I_i \in \mathbb{R};\ \theta_i \in \mathbb{T};\ i = 1, 2$$

to possesses a resonant normally parabolic torus at the origin are:

c1. The fixed point conditions:

$$\nabla_{(x,y)} H_0(0, 0, I_1, I_2) = (0, 0). \tag{12}$$

c2. The parabolicity conditions:

$$\det\left(\frac{\partial^2 H_0(x, y, I_1, I_2)}{(\partial x, \partial y)}|_{(0,0,0,I_2)}\right) = 0. \tag{13}$$

c3. The condition on the inner frequencies of the parabolic 2-torus for a 1-resonance, corresponding to some pair $(n, m) \in \mathbb{Z}^2 \backslash \{0, 0\}$, is:

$$n\dot{\theta}_1 + m\dot{\theta}_2 = n\frac{\partial H_0}{\partial I_1}|_{(0,0,0,0)} + m\frac{\partial H_0}{\partial I_2}|_{(0,0,0,0)} = 0. \tag{14}$$

Since a 2-torus may fulfill at most two independent resonance conditions (a 2-resonance), the two independent pairs of integers may be chosen WNLG to be $(n, 0)$ and $(0, m)$[8]. The condition for a 1-resonance, corresponding to the pair $(n, 0)$, $n \in \mathbb{Z}\backslash\{0\}$, is:

$$\dot{\theta}_1 = \frac{\partial H_0(x, y, I_1, I_2)}{\partial I_1}|_{(0,0,0,0)} = 0. \tag{15}$$

Similarly, the condition for a 1-resonance, corresponding to the pair $(0, m)$, $m \in \mathbb{Z}\backslash\{0\}$, is:

$$\dot{\theta}_2 = \frac{\partial H_0(x, y, I_1, I_2)}{\partial I_2}|_{(0,0,0,\bar{I}_2)} = 0. \tag{16}$$

[8]If some two general independent vectors of integers are chosen, the two corresponding resonance conditions may be replaced by the conditions (15) and (16) by a simplectic change of coordinates.

For achieving a 2-resonance, we need the conditions (15) and (16) to be fulfilled simultaneously on the parabolic torus. Obviously, an external parameter is needed for the 2-resonance condition, let us denote this parameter by α_2:

- **c4.** The condition on the inner frequencies of the parabolic 2-torus for a 2-resonance, corresponding to the pairs $(n, 0)$ and $(0, m)$, for some $n, m \in \mathbb{Z}\backslash\{0\}$, is:

$$\nabla_{(I_1,I_2)} H_0(0,0,0,I_2=\alpha_2;\alpha_2=0) = (\dot{\theta}_1, \dot{\theta}_2)|_{(0,0,0,0;0)} = (0,0). \quad (17)$$

The phenomenological model (2) clearly satisfies the conditions (15), (16) for a 1-resonance in I_1 direction (a 2-torus of closed orbits periodic in θ_2) and a 1-resonance in I_2 direction (a 2-torus of closed orbits periodic in θ_1), respectively. Similarly, it satisfies the condition (17) for a 2-resonance which corresponds to a 2-torus of fixed points.

To further simplify the model, we add the following assumptions on the near integrable Hamiltonian H:

- **a1.** The Hamiltonian is of the form:

$$H(x, y, \theta_1, I_1, \theta_2, I_2) = \frac{y^2}{2} + V(x, I_1, I_2) + O([I_1, I_2]^3, 5),$$

  where V is the potential of the unperturbed system; i.e. the terms in V to order 4 are independent of y and of θ_1, θ_2.

- **a2.** The action I_1 governs the stability type of the system linearized at the two dimensional torus corresponding to the equilibrium at the origin of the (x, y) plane, O_{xy}; i.e. it serves like a bifurcation parameter. The action I_2 governs the creation of 1-resonances, and together with the external parameter, α_2, it is responsible for the existence of 2-resonances.

- **a3.** All the energy surfaces of the Hamiltonian are compact in the (x, y) plane.

- **a4.** The unstable fixed point, which is created by the pitchfork bifurcation in the (x, y) plane, is shifted to the origin for all I_1, I_2 for which it exists.

Assumption a1 corresponds to assuming that the Hamiltonian is in the standard form for mechanical Hamiltonian systems which are integrable to quartic order. Assumption a2 is made for simplicity, and seems to have no effect on the behavior of the system. Moreover, when only the integrable part of the Hamiltonian, H_0, is considered, assumption a2 is achieved by a simplectic change of variables. Assumption a3 corresponds to considering the large class of Hamiltonian systems for which the motion in the (x, y) plane must be bounded. Assumption a4 is made WNLG, and it may be always achieved by a local change of coordinates. Note that under assumptions a1 and a2, the parabolicity condition, c2, may be written in the form:

$$\det\left(\frac{\partial^2 V(x, y, I_1, I_2)}{\partial x^2}\Big|_{(0,0,0,I_2)}\right) = 0; \quad I_2 \in \mathbb{R}. \tag{18}$$

Making a Taylor expansion near the above conditions, rescaling and using the above assumptions result with the Hamiltonian function in equations (1) in section 2.

B Allowed regions of motion

Details of the calculations which lead to identifying the allowed regions of motion in the space of constants of motion of the system (2) are presented for the case $\eta = 0$, $\alpha_1 > -\frac{1}{2}$, and $\alpha_3 \geq 0$. When $\eta = 0$, the integrable Hamiltonian of the system (2) is:

$$H_0(x, y, I; \mu) = \frac{y^2}{2} - I_1\frac{x^2}{2} + \frac{x^4}{4} + \alpha_2 I_2 + (\frac{1}{2} + \alpha_1)\frac{I_1^2}{2} + \frac{I_2^2}{2} + \alpha_3 I_1 I_2 \tag{19}$$

Since equilibria of the (x, y) system supply boundaries to the energy surfaces of the full system, we find the energy values (equation (19)) at these points. The fixed points of the integrable system (2) in the (x, y) plane, for $\eta = 0$, are: $(0, 0)$ ($I_1 < 0$ - elliptic; $I_1 = 0$ - parabolic; $I_1 > 0$ - hyperbolic) and $(\pm\sqrt{I_1}, 0)$ ($I_1 > 0$ - elliptic).

The origin of the (x, y) plane, O_{xy}, is a fixed point for any value of I_1 and I_2. At O_{xy}, (19) may be solved for I_1:

$$I_{1_{O_{xy}\pm}}(H_0, I_2) = \frac{-2\alpha_3 I_2 \pm 2\sqrt{\alpha_3^2 I_2^2 - (1 + 2\alpha_1)(\alpha_2 I_2 + \frac{I_2^2}{2} - H_0)}}{1 + 2\alpha_1}. \tag{20}$$

For each fixed value of I_2, the curves $I_{1_{O_{xy}-}}(H_0, I_2)$ and $I_{1_{O_{xy}+}}(H_0, I_2)$ form horizontal parabolas in the space (H_0, I_2, I_1). In the energy-actions bifurcation diagrams, presented in section 2.1, figures 1 - 9, these equilibria curves appear as solid curves if they refer to a stable equilibrium, and they appear as dashed curves, if they refer to an unstable equilibrium (and separatrix). The minimal possible value of $H_0(I_2)$, for which the manifolds (20) are defined, is found by solving the equation:

$$\frac{\partial H_0}{\partial I_1}|_{O_{xy}} = 0. \tag{21}$$

Notice that $\frac{\partial H_0}{\partial I_1}|_{O_{xy}} = \dot{\theta}_1|_{O_{xy}}$, hence for I_1 values which solve equation (21), an $(n, 0)$ resonance occurs with respect to the inner frequencies of the corresponding 2-tori. These $I_{1_{res1}}$ values are:

$$I_{1_{res1}}(I_2) = \frac{-2\alpha_3 I_2}{1 + 2\alpha_1}. \tag{22}$$

Substituting (22) into equation (19) at O_{xy} one gets:

$$H_{0_{O_{xy}-\min}}(I_2) = \alpha_2 I_2 + (\frac{1}{2} - \frac{\alpha_3^2}{1 + 2\alpha_1})I_2^2, \tag{23}$$

Which is the minimal energy value that should be considered at O_{xy}. Hence, the point $(H_{0_{O_{xy}-\min}}(I_2), I_{1_{res1}}(I_2))$, obtained from equations (22) and (23), is the minimal point of the parabolas formed by equation (20) for each fixed value of I_2.

When $I_1 > 0$, O_{xy} is a hyperbolic fixed point in the (x, y) plane (for any value of I_2). The energy value at the parabolic surface $(I_1 = 0)$ is:

$$H_{0_p}(I_2) = \alpha_2 I_2 + \frac{I_2^2}{2}. \tag{24}$$

Notice that at O_{xyI_1} $((x, y, I_1, I_2) = (0, 0, 0, I_2))$ this energy value corresponds to a normally parabolic torus in the full phase space. When I_1 turns to be positive, in addition to the hyperbolic equilibrium at the origin, two elliptic fixed points appear in the (x, y) plane:

$$(x_{ell}, y_{ell}) = (\pm\sqrt{I_1}, 0). \tag{25}$$

Substituting (25) into (19) one gets:

$$H_{0_{ell}}(I_1, I_2) = \alpha_2 I_2 + \alpha_1 \frac{I_1^2}{2} + \frac{I_2^2}{2} + \alpha_3 I_1 I_2. \tag{26}$$

Equation (26) may be solved for I_1:

$$I_{1_{ell\pm}}(H_0, I_2) = \frac{-\alpha_3 I_2 \pm \sqrt{I_2^2(\alpha_3^2 - \alpha_1) - 2\alpha_1\alpha_2 I_2 + 2\alpha_1 H_0}}{\alpha 1}. \tag{27}$$

For each fixed value of I_2, the curves from equation (27) may be seen in figures 1 - 9 as solid curves for positive values of I_1, as they denote elliptic equilibria. For $\alpha_1 > 0$ ($-\frac{1}{2} < \alpha_1 < 0$) the minimal (maximal) energy value, for which the manifolds in equation (27) are defined, is:

$$H_{0_{ell-\min}}(I_2) = \alpha_2 I_2 + (\frac{1}{2} - \frac{\alpha_3^2}{2\alpha_1})I_2^2, \tag{28}$$

and it is achieved at:

$$I_{1_{ell\_res}}(I_2) = \frac{-\alpha_3 I_2}{\alpha_1}. \tag{29}$$

However, the manifolds $I_{1_{ell\pm}}(H_0, I_2)$ are defined only when the right hand side of (27) is positive. Hence, $H_{0_{ell-\min}}(I_2)$ is their minimal ($\alpha_1 > 0$) or maximal ($-\frac{1}{2} < \alpha_1 < 0$) energy value only if α_1 and I_2 are of opposite signs. Otherwise, their minimal ($\alpha_1 > 0$) or maximal ($-\frac{1}{2} < \alpha_1 < 0$) energy value is $H_{0_p}(I_2)$ (equation (24)). Notice that when α_1 and I_2 are of opposite signs, and $I_1 = I_{1_{ell\_res}}(I_2)$ (from equation (29)), the elliptic fixed points in the (x, y) plane correspond to normally elliptic resonant tori in the full phase space (for the same reasoning like above for O_{xy}).

When $\alpha_1 = 0$ the manifolds (27) cease to exist. For $I_2 \neq 0$ they are replaced by the manifold:

$$I_{1_{ell0}}(H_0, I_2) = \frac{2H_0 - 2\alpha_2 I_2 - I_2^2}{2\alpha_3 I_2}, \tag{30}$$

and for $I_2 = 0$ they are replaced by the line $H_0 \equiv 0$. Since for each fixed value of I_2, the curves in (27), (30), and the line $H_0 \equiv 0$, refer to a stable equilibrium, they are denoted by solid curves in the bifurcation diagrams, presented in section 2.1, figures 6:a,c and 6:b, respectively.

Now let us determine which is the minimal energy value, when such exists, that should be considered for different parameters and variables values. First of all, let as note that when $\alpha_1 \geq 0$ (or when $\alpha_1 \leq -0.5$), $H_{0_{ell-\min}}(I_2) \leq H_{0_{O_{xy}-\min}}(I_2)$, and when $-0.5 \leq \alpha_1 \leq 0$, $H_{0_{O_{xy}-\min}}(I_2) \leq H_{0_{ell-\min}}(I_2)$. As the next step, we continue to determine the domain of definition of the Hamiltonian equation (19). Equation (19) may be rewritten in the form:

$$\frac{y^2}{2} = H_0 + I_1\frac{x^2}{2} - \frac{x^4}{4} - \alpha_2 I_2 - (\frac{1}{2} + \alpha_1)\frac{I_1^2}{2} - \frac{I_2^2}{2} - \alpha_3 I_1 I_2, \tag{31}$$

which imply that the right hand side of (31) must be nonnegative. When $x=0$, the right hand side of (31) is nonnegative for:

$$I_1 \in [I_{1_{Oxy-}}(H_0, I_2), I_{1_{Oxy+}}(H_0, I_2)], \tag{32}$$

($I_{1_{Oxy\pm}}(H_0, I_2)$ are as in (20)). Moreover, it follows from (31) that for $\alpha_1 \geq 0$ and $I_2 \geq 0$, $H_{0_{Oxy-\min}}(I_2)$ (equation (23)) is the minimal energy value that should be considered: i.e., when $I_{1_{res1}}(I_2) \leq 0$, $H_{0_{Oxy-\min}}(I_2)$ is the minimal energy value for which motion is allowed. See for example figure 5:a. Note that if $I_{1_{res1}}(I_2) < 0$, the points $(H_0, I_2, I_1) = (H_{0_{Oxy-\min}}(I_2), I_2, I_{1_{res1}}(I_2))$ correspond to elliptic resonant tori, and if $I_{1_{res1}}(0) = 0$, the point $(H_0, I_2, I_1) = (0, 0, 0)$ corresponds to a parabolic resonant torus. See for example figure 5:b. When $x = \pm\sqrt{I_1}$, $\alpha_1 \geq 0$ and $I_2 < 0$, the right hand side of (31) is nonnegative for:

$$I_1 \in [I_{1_{ell-}}(H_0, I_2), I_{1_{elll+}}(H_0, I_2)], \tag{33}$$

for positive I_1 values, there the manifolds (27) are defined. Moreover, it follows from equation (31), that $H_{0_{ell-\min}}(I_2)$ is the minimal energy value that should be considered for $\alpha_1 > 0$ and $I_2 < 0$ (see figure 5:c).

Continuing with similar considerations we conclude: For $\alpha_1 > 0$, the minimal energy value for which motion is allowed is $H_{0_{Oxy-\min}}(I_2)$ when $I_2 \geq 0$, and $H_{0_{ell-\min}}(I_2)$ when $I_2 < 0$. For $\alpha_1 = 0$, the minimal energy value is $H_{0_{Oxy-\min}}(I_2)$ when $I_2 \geq 0$. For $\alpha_1 = 0$ and $I_2 < 0$, and for $-\frac{1}{2} < \alpha_1 < 0$ and any value of I_2, minimal energy value does not exist, and motion is allowed for *all* energy values. See for example figure 7 in section 2.1.

For the considered parameters values, the energy surfaces are always bounded from below in I_1 direction. The bounding manifold from below in I_1 direction may be either one of the manifolds: $I_{1_{Oxy-}}(H_0, I_2)$, $I_{1_{ell-}}(H_0, I_2)$, $I_{1_{ell0}}(H_0, I_2)$, depending on the range of energy, I_2 and α_1 values (for each fixed triple (H_0, I_2, α_1) only one of these is defined). For $\alpha_1 > 0$ the energy surfaces are bounded from above in I_1 direction: When $I_2 \geq 0$, the upper bound is either the *stable part* of $I_{1_{Oxy+}}(H_0, I_2)$ or of $I_{1_{ell+}}(H_0, I_2)$, depending on the range of the energy values (again, for each energy value, only one of these exists). When $I_2 < 0$, the upper bound is $I_{1_{ell+}}(H_0, I_2)$ for all allowed energy values. For $\alpha_1 = 0$, the energy surfaces are bounded from above in I_1 direction only for positive I_2 values, by the manifold $I_{1_{ell0}}(H_0, I_2)$. For all other values of α_1 and of I_2, the energy surfaces are unbounded from above in I_1 direction. The regions of allowed motion between or above the equilibria bounds are denoted by vertical lines in figures 5 - 7 in section 2.1.

See table 1 for a summary and full description of the regions in (H_0, I_2, I_1) space where motion is allowed for different values of the parameter α_1.

Remark 1 *In all the tables, for simplicity of notation, we use:* $H_{0_{Oxy-\min}} := H_{0_{Oxy-\min}}(I_2)$, $H_{0_p} := H_{0_p}(I_2)$, $H_{0_{ell-\min}} := H_{0_{ell-\min}}(I_2)$, $I_{1_{Oxy\pm}} := I_{1_{Oxy\pm}}(H_0, I_2)$, $I_{1_{ell\pm,0}} := I_{1_{ell\pm,0}}(H_0, I_2)$, $I_{1_{\Delta\pm,0}} := I_{1_{\Delta\pm,0}}(H_0, I_2)$, $I_{1_{res1}} := I_{1_{res1}}(I_2)$.

	$\alpha_1 > 0$	$\alpha_1 = 0$	$-\frac{1}{2} < \alpha_1 < 0$
$I_2 > 0$	$H_0 \in [H_{0_{Oxy-\min}}, H_{0_p}]$ $\Rightarrow I_1 \in [I_{1_{Oxy-}}, I_{1_{Oxy+}}]$, $H_0 \geq H_{0_p}$ $\Rightarrow I_1 \in [I_{1_{Oxy-}}, I_{1_{ell+}}]$	$H_0 \in [H_{0_{Oxy-\min}}, H_{0_p}]$ $\Rightarrow I_1 \in [I_{1_{Oxy-}}, I_{1_{Oxy+}}]$, $H_0 \geq H_{0_p}$ $\Rightarrow I_1 \in [I_{1_{Oxy-}}, I_{1_{ell0}}]$	$H_0 \leq H_{0_{Oxy-\min}}$ $\Rightarrow I_1 \in [I_{1_{ell-}}, \infty)$, $H_0 \in [H_{0_{Oxy-\min}}, H_{0_p}]$ $\Rightarrow I_1 \in [I_{1_{Oxy-}}, I_{1_{Oxy+}}]$ $\cup$ $[I_{1_{ell-}}, \infty)$, $H_0 \geq H_{0_p}$ $\Rightarrow I_1 \in [I_{1_{Oxy-}}, \infty)$
$I_2 = 0$	$H_0 \geq 0$ $\Rightarrow I_1 \in [I_{1_{Oxy-}}, I_{1_{ell+}}]$	$H_0 \geq 0$ $\Rightarrow I_1 \in [I_{1_{Oxy-}}, \infty)$	$H_0 \leq 0$ $\Rightarrow I_1 \in [I_{1_{ell-}}, \infty)$, $H_0 \geq 0$ $\Rightarrow I_1 \in [I_{1_{Oxy-}}, \infty)$
$I_2 < 0$	$H_0 \in [H_{0_{ell-\min}}, H_{0_p}]$ $\Rightarrow I_1 \in [I_{1_{ell-}}, I_{1_{ell+}}]$, $H_0 \geq H_{0_p}$ $\Rightarrow I_1 \in [I_{1_{Oxy-}}, I_{1_{ell+}}]$	$H_0 \leq H_{0_{Oxy-\min}}$ $\Rightarrow I_1 \in [I_{1_{ell0}}, \infty)$, $H_0 \in [H_{0_{Oxy-\min}}, H_{0_p}]$ $\Rightarrow I_1 \in [I_{1_{Oxy-}}, I_{1_{Oxy+}}]$ $\cup$ $[I_{1_{ell0}}, \infty)$, $H_0 \geq H_{0_p}$ $\Rightarrow I_1 \in [I_{1_{Oxy-}}, \infty)$	$H_0 \leq H_{0_p}$ $\Rightarrow I_1 \in [I_{1_{ell-}}, \infty)$, $H_0 \geq H_{0_p}$ $\Rightarrow I_1 \in [I_{1_{Oxy-}}, \infty)$

Table 1: The domain of definition of the integrable Hamiltonian equation - allowed regions of motion.

The regions of allowed motion are calculated for constructing the energy-momenta bifurcations diagrams by fixing a value of I_2, and then obtaining the range of the allowed values of H_0 and I_1 for which the Hamiltonian equation is well defined. On the other hand, if specific energy surface is to be analyzed, one may want to fix the energy value and to obtain the allowed values of I_1 and I_2 for which the Hamiltonian is defined on this particular energy surface.

The curves defining the region(s) of I_2 values, for a fixed energy value, H_0, and such that the I_1 values are defined by the curves: $I_{1_{Oxy\pm}}(H_0, I_2)$ and $I_{1_{ell\pm}}(H_0, I_2)$ (equations (20, 27)), calculated above, are:

$$I_{2_{Oxy\pm}} = \frac{-(1+2\alpha_1)\alpha_2 \pm \sqrt{\alpha_2^2(1+2\alpha_1)^2 + 4(-\alpha_3^2 + 0.5 + \alpha_1)(1+2\alpha_1)H_0}}{1+2\alpha_1 - 2\alpha_3^2}, \tag{34}$$

which define for $\alpha_1 - \alpha_3^2 \neq -\frac{1}{2}$ a parabola attaining its maxima (for $\alpha_1 - \alpha_3^2 < -\frac{1}{2}$) or minima (for $\alpha_1 - \alpha_3^2 > -\frac{1}{2}$) at the critical value of H_0:

$$H_{0_{gm\pm}} = -\frac{\alpha_2^2(1+2\alpha_1)}{2(1+2(\alpha_1 - \alpha_3^2))}, \tag{35}$$

and:

$$I_{2_{ell\pm}} = \frac{-\alpha_1\alpha_2 \pm \sqrt{(\alpha_1\alpha_2)^2 + 2(-\alpha_3^2 + \alpha_1)\alpha_1 H0}}{\alpha_1 - \alpha_3^2}, \tag{36}$$

which define for $\alpha_1 - \alpha_3^2 \neq 0$ a parabola attaining its maxima (for $\alpha_1 - \alpha_3^2 < 0$) or minima (for $\alpha_1 - \alpha_3^2 > 0$) at the critical value of H_0:

$$H_{0_{gm-ell}} = -\frac{\alpha_1\alpha_2^2}{2(\alpha_1 - \alpha_3^2)}. \tag{37}$$

For the parameter values for which these parabolas attaining minima, the values of I_2 for which the corresponding parabolas defining the values of I_1 (equations (20, 27)), for a given energy value, H_0, are defined inside the parabola. Hence the corresponding energy surface is continuous and bounded in I_2 if $H_0 \geq H_{0_{gm-ell}}$, and there are no values of I_2 for which motion is allowed if $H_0 < H_{0_{gm-ell}}$ (i.e. no energy surface exists for this value of H_0). When both parabolas attaining a maxima, the energy surface is unbounded in I_2 (as then the allowed I_2 values are outside the parabolas), where for energy values $H_0 \geq H_{0_{gm\pm}}$ the energy surface is defined for all I_2 values, and for $H_0 < H_{0_{gm\pm}}$ the corresponding energy surface may be connected, or disconnected, in I_2. When $-\frac{1}{2} < \alpha_1 - \alpha_3^2 < 0$, and (34) attaining a minima and (36) attaining a maxima the energy surfaces behave in a similar way. At the degenerate points, for which these parabolas cease to exist, lines which define the allowed I_2 values, replace the parabolas (34) and (36). At the degenerate points flat PRs appear for certain values of I_2.

C Regions of backflow

Here we seek I_1 values for which backflow occurs in the allowed regions of motion. i.e. we seek values of I_1 for which the right hand side of equation (31) is nonnegative, and $\dot{\theta}_1 = 0$. At O_{xy}, $\dot{\theta}_1 = 0$ for $I_{1_{res1}}(I_2)$ (equation (22)). Assuming that $\dot{\theta}_1 = 0$ for some x value, x^2 may be eliminated from the third equation of the integrable system (2):

$$x_{res}{}^2(I_1, I_2) = (1 + 2\alpha_1)I_1 + 2\alpha_3 I_2. \tag{38}$$

Hence, $\dot{\theta}_1$ may vanish only when the right hand side of equation (38) is nonnegative. Therefore, it follows that $\dot{\theta}_1$ may change sign along orbits only if $I_1 \geq I_{1_{res1}}(I_2)$. Substituting (38) into the right hand side of (31) and solving for I_1 one gets:

$$I_{1_{\Delta\pm}}(H_0, I_2) = \frac{-\alpha_3 I_2}{\alpha_1} \pm \frac{\sqrt{\alpha_3^2 I_2^2 + \alpha_1(2H_0 - I_2(2\alpha_2 + I_2))}}{\alpha_1\sqrt{1 + 2\alpha_1}}, \tag{39}$$

where $I_1 \in [I_{1_{\Delta-}}(H_0, I_2), I_{1_{\Delta+}}(H_0, I_2)]$ if $\alpha_1 > 0$ and $I_1 \in]I_{1_{\Delta+}}(H_0, I_2), I_{1_{\Delta-}}(H_0, I_2)[$ if $-\frac{1}{2} < \alpha_1 < 0$. These manifolds are defined for $H_0 \geq H_{0_{ell-\min}}$ when $\alpha_1 > 0$, and for $H_0 \leq H_{0_{ell-\min}}$ when $-\frac{1}{2} < \alpha_1 < 0$. They cease to exist when $\alpha_1 = 0$, where they are replaced by the manifold:

$$I_{1_{\Delta 0}}(H_0, I_2) = \frac{H_0 - \alpha_2 I_2 - I_2^2(\frac{1}{2} + \alpha_3^2)}{\alpha_3 I_2}, \tag{40}$$

where $I_1 \leq I_{1_{\Delta 0}}(H_0, I_2)$ for $I_2 > 0$ and $I_1 \geq I_{1_{\Delta 0}}(H_0, I_2)$ for $I_2 < 0$. For $\alpha_1 = I_2 = 0$ non of these manifolds is defined.

Hence, backflow occurs for I_1 values which are in the specified above ranges, and are greater or equal to $I_1 = I_{1_{res1}}(I_2)$. The summary of where $\dot{\theta}_1$ changes its sign on a given energy surface is given in table 2 (the shaded area in figures 1 - 9).

Note that when $\dot{\theta}_1$ vanishes on an equilibrium point of the (x, y) plane, a resonance occurs. It happens for $I_1 = I_{1_{res1}}(I_2)$ (equation (22)) at O_{xy},

	$\alpha_1 > 0$	$\alpha_1 = 0$	$-\frac{1}{2} < \alpha_1 < 0$
$I_2 > 0$	$I_1 \in [I_{1_{res1}}, I_{1_{\Delta+}}]$	$I_1 \in [I_{1_{res1}}, I_{1_{\Delta 0}}]$	$H_0 \leq H_{0_{end}} \Rightarrow$ $I_1 \in [I_{1_{res1}}, I_{1_{\Delta+}}]$ $\cup \quad [I_{1_{\Delta-}}, \infty)$, $H_0 \geq H_{0_{end}} \Rightarrow$ $I_1 \in [I_{1_{res1}}, \infty)$
$I_2 = 0$	$I_1 \in [I_{1_{res1}}, I_{1_{\Delta+}}]$	$I_1 \in [I_{1_{res1}}, \infty)$	$H_0 \leq H_{0_{min}} \Rightarrow$ $I_1 \in [I_{1_{\Delta-}}, \infty)$, $H_0 \geq H_{0_{min}} \Rightarrow$ $I_1 \in [I_{1_{res1}}, \infty)$
$I_2 < 0$	$H_0 \in [H_{0_{end}}, H_{0_{min}}]$ $\Rightarrow I_1 \in [I_{1_{\Delta-}}, I_{1_{\Delta+}}]$, $H_0 \geq H_{0_{min}}$ $\Rightarrow I_1 \in [I_{1_{res1}}, I_{1_{\Delta+}}]$	$H_0 \leq H_{0_{min}} \Rightarrow$ $I_1 \in [I_{1_{\Delta 0}}, \infty)$, $H_0 \geq H_{0_{min}} \Rightarrow$ $I_1 \in [I_{1_{res1}}, \infty)$	$H_0 \leq H_{0_{min}} \Rightarrow$ $I_1 \in [I_{1_{\Delta-}}, \infty)$, $H_0 \geq H_{0_{min}} \Rightarrow$ $I_1 \in [I_{1_{res1}}, \infty)$

Table 2: The regions where $\dot{\theta}_1$ changes sign and backflow occurs.

and if α_1 and I_2 are of opposite signs, for $I_1 = I_{1_{ell\_res}}(I_2)$ (equation (29)) at $(x, y) = (\pm\sqrt{I_1}, 0)$. We denote these resonance values of I_1 by asterisks in the bifurcation diagrams presented in figures 1 - 9, in section 2.1.

On a given energy surface, $\dot{\theta}_1$ vanishes on the separatrix if:

- $I_2 > 0, H_0 \geq H_{0_p}(I_2)$ and:

  $\alpha_1 > 0$; $I_{1_{\Delta+}}(H_0, I_2) \geq I_{1_{O_{xy}+}}(H_0, I_2)$ or

  $-\frac{1}{2} < \alpha_1 < 0$; $I_{1_{\Delta-}}(H_0, I_2) \geq I_{1_{O_{xy}+}}(H_0, I_2)$ or

  $\alpha_1 = 0$; $I_{1_{\Delta 0}}(H_0, I_2) \geq I_{1_{O_{xy}+}}(H_0, I_2)$,

- $I_2 < 0$ and:

  $\alpha_1 > 0$; $I_{1_{\Delta+}}(H_0, I_2) \geq I_{1_{O_{xy}+}}(H_0, I_2)$ or

  $-\frac{1}{2} < \alpha_1 < 0$; $I_{1_{\Delta-}}(H_0, I_2) \geq I_{1_{O_{xy}+}}(H_0, I_2)$ or

  $\alpha_1 = 0$; $I_{1_{\Delta 0}}(H_0, I_2) \geq I_{1_{O_{xy}+}}(H_0, I_2)$,

- $I_2 = 0$ and:

  $\alpha_1 > 0$; $I_{1_{\Delta+}}(H_0, I_2) \geq I_{1_{O_{xy}+}}(H_0, I_2)$ or

  $-\frac{1}{2} < \alpha_1 < 0$; $I_{1_{\Delta-}}(H_0, I_2) \geq I_{1_{O_{xy}+}}(H_0, I_2)$ or

  $\alpha_1 = 0$.

References

[1] V. I. Arnol'd. Proof of a theorem of A. N. Kolmogorov on the invariance of quasi-periodic motions under small perturbations of the Hamiltonian. *Russ. Math. Surv.*, 18(5):9–36, 1963.

[2] V. I. Arnol'd. *Mathematical Methods of Classical Mechanics*. Springer, 1978.

[3] V. I. Arnol'd. *Dynamical Systems III*, volume 3 of *Encyclopedia of Mathematical Sciences*. Springer-Verlag, second edition, 1993.

[4] N. Fenichel. Persistence and smoothness of invariant manifolds for flows. *Ind. Univ. Math. J.*, 21:193–225, 1971.

[5] S. M. Graff. On the conservation of hyperbolic invariant tori for Hamiltonian systems. *J. Diff. Eq.*, 15:1–69, 1974.

[6] G. Haller. *Chaos Near Resonance*. Applied Mathematical Sciences; 138. Springer-Verlag, NY, 1999.

[7] G. Haller and S. Wiggins. Multi-pulse jumping orbits and homoclinic trees in a modal truncation of the damped-forced nonlinear schrödinger equation. *Physica D*, 85(3):311–347, 1995.

[8] G. Haller and S. Wiggins. Geometry and chaos near resonant equilibria of 3-d.o.f. Hamiltonian systems. *Physica D*, 90(4):319–365, 1996.

[9] H. Handßmann. The quasi-periodic center-saddle bifurcation. *Journal of Differential Equations*, 142(2):305–370, January 1997.

[10] N. Lebovitz and A. Pesci. Dynamics bifurcation in Hamiltonian systems with one degree of freedom. *SIAM J. Appl. Math.*, 55(4):1117–1133, 1995.

[11] A. Litvak-Hinenzon and V. Rom-Kedar. Resonant tori and instabilities in Hamiltonian systems. In preparation, to be submitted to Nonlinearity; "Parabolic Resonance in Near Integrable Hamiltonian Systems", in *Stochaos: Stochastic and Chaotic Dynamics in the Lakes*, Broomhead, D. S. , Luchinskaya, E. A., McClintock, P V E, Mullin, T eds, pp 358-368, 2000, American Institute of Physics, Woodbury, NY; "Parabolic resonances in near integrable Hamiltonian systems", PhD thesis, Weizmann Institute, submitted September 2000.

[12] G. Mareé. Slow passage through a pitchfork bifurcation. *SIAM J. Appl. Math.*, 56(3):889–918, 1996.

[13] N. Paldor and E. Boss. Chaotic trajectories of tidally perturbed inertial oscillations. *J. Atmos. Sci.*, 49:2306–2318, 1992.

[14] J. Pöschel. On elliptic lower dimensional tori in Hamiltonian systems. *Math. Z.*, 202:559–608, 1989.

[15] V. Rom-Kedar. Parabolic resonances and instabilities. *Chaos*, 7(1):148–158, 1997.

[16] V. Rom-Kedar, Y. Dvorkin, and N. Paldor. Chaotic Hamiltonian dynamics of particle's horizontal motion in the atmosphere. *Physica D*, 106:389–431, 1997.

[17] V. Rom-Kedar and N. Paldor. From the tropics to the poles in forty days. *Bulletin of the American Meteorological Society*, 78(12):2779–2784, December 1997.

[18] G. Zaslavsky, R. Sagdeev, D. Usikov, and A. Chernikov. Minimal chaos, stochastic webs and structures of quasicrystal symmetry. *Sov. Phys. Usp.*, 31(10), 1988. and references therein.